AJAE

Open Access

Vol. 15, No. 2, 2021008, June 2021
doi: https://doi.org/10.5572/ajae.2021.008
ISSN (Online) 2287-1160, ISSN (Print) 1976-6912

Research Article

# Advantages of Continuous Monitoring of Hourly $PM_{2.5}$ Component Concentrations in Japan for Model Validation and Source Sensitivity Analyses

**Satoru Chatani*, Syuichi Itahashi[1)], Kazuyo Yamaji[2)]**

National Institute for Environmental Studies, Tsukuba, Ibaraki 305-8506, Japan
[1)]Central Research Institute of Electric Power Industry, Abiko, Chiba 270-1194, Japan
[2)]Kobe University, Kobe, Hyogo 658-0022, Japan

***Corresponding author.**
Tel: +81-29-850-2740
E-mail: chatani.satoru@nies.go.jp

**Received:** 15 January 2021
**Revised:** 19 March 2021
**Accepted:** 28 April 2021

**ABSTRACT** Continuous monitoring of hourly $PM_{2.5}$ component concentrations has been performed in Japan. The objective of this study was to evaluate the advantages of continuous monitoring to obtain data that can be useful for regional air quality simulations. Inclusion of transboundary transport in the simulations improved the correlation between the observed and simulated hourly concentrations of $SO_4^{2-}$, $NO_3^-$, secondary organic aerosols (SOA), and metals in $PM_{2.5}$. Black carbon was an exception, suggesting the overestimation of emissions in upwind countries. Including volcanic and dust emissions also improved the correlations between the observed and simulated hourly concentrations of $SO_4^{2-}$ and metals, respectively. However, despite the good correlation achieved by including transboundary transport, it also resulted in overestimated $NO_3^-$ and SOA concentrations in western Japan during the winter. Further improvements are necessary, such as balancing with $SO_4^{2-}$ and the dry deposition of gaseous $HNO_3$ for $NO_3^-$, and new treatment of the partitioning and aging of semivolatile organic aerosols, which have been incorporated into recent models for SOA. The differences in model performance with regard to simulating metal concentrations suggest imbalances in the speciation profiles used for countries other than Japan. Further, comparing the observed and simulated hourly concentrations helped identify the key processes driving air quality. This revealed evening peaks in black carbon concentrations, owing to the relatively stable atmosphere; and early morning peaks in $NO_3^-$ concentration, owing to the low temperature and high humidity through thermodynamic equilibrium. This study demonstrated that continuous monitoring of hourly variations in $PM_{2.5}$ composition is valuable for understanding the roles of the emission sources and for improving future models, both of which contribute to deriving effective $PM_{2.5}$ suppression strategies.

**KEY WORDS** $PM_{2.5}$ composition, Regional air quality simulation, Continuous monitoring, Hourly variation, Source sensitivity

## 1. INTRODUCTION

Fine particulate matter smaller than 2.5 μm ($PM_{2.5}$) adversely affects human health (Kojima *et al.*, 2020). The Environmental Quality Standard for $PM_{2.5}$ was introduced in Japan in 2009. Despite various strategies that have been implemented,

ambient $PM_{2.5}$ concentrations still exceed this standard at some of the monitoring stations in Japan (Ministry of the Environment, 2020).

$PM_{2.5}$ consists of multiple components: its primary components are emitted directly from the source as particulates, while secondary components form in the atmosphere from gaseous precursors via photochemical reactions. There are many different emission sources of primary components, and gaseous precursors of secondary components. Therefore, it is essential to clarify the $PM_{2.5}$ composition to develop effective mitigation strategies for reducing emissions from key contributing sources.

In addition to the routine monitoring of $PM_{2.5}$ mass concentrations at general monitoring stations, the Ministry of the Environment of Japan (MOEJ) has initiated a $PM_{2.5}$ composition monitoring campaign in cooperation with local governments. As part of this campaign, daily variations in the concentrations of $PM_{2.5}$ components collected on filters are measured for two weeks in each season. During the 2018 fiscal year, monitoring was conducted at 179 locations throughout Japan (Ministry of the Environment, 2020). These measurement data have been utilized in various scientific studies, including validation of regional air quality simulations (Itahashi *et al.*, 2020b; Yamaji *et al.*, 2020; Itahashi *et al.*, 2018a; Uranishi *et al.*, 2017). Such simulations are useful for investigating the relationships between emission sources and ambient $PM_{2.5}$ concentration, taking photochemical reactions into account. However, one of the disadvantages of this monitoring campaign is that it is restricted to only two weeks per season, with daily averaged samples. Therefore, the data may not reflect the typical air quality during the respective seasons. Moreover, the variations in the daily averages may be insufficient to fully understand the dynamic behavior of individual $PM_{2.5}$ components.

To overcome these disadvantages, the MOEJ has begun automated continuous monitoring of hourly $PM_{2.5}$ component concentrations. It has several advantages. Hourly variations obtained in this monitoring are helpful for understanding the dynamic behavior of $PM_{2.5}$ components. Using a short sampling duration is effective at suppressing any loss of $PM_{2.5}$ components caused by evaporation from the samples. Continuous monitoring does not miss elevated concentrations of $PM_{2.5}$ components that may occur throughout the year. In addition, some of the components identified in this monitoring are not available in conventional monitoring data. Monitoring conducted at multiple locations also enables the understanding of spatial variations in $PM_{2.5}$ components. The objective of this study was to evaluate how these advantages of the continuous monitoring of $PM_{2.5}$ compositions are effective for regional air quality simulations. This data has previously been analyzed by only a few studies, and for limited time periods (Itahashi *et al.*, 2020a). Herein, we conducted the first comprehensive analysis of this data for the entire year. We validated hourly $PM_{2.5}$ component concentrations simulated by three different regional chemical transport models in comparisons with those obtained in the monitoring. In addition, we investigated the influences of key emission sources on hourly variations in the observed and simulated $PM_{2.5}$ component concentrations. Through these investigations, we evaluated the effectiveness of the continuous monitoring of $PM_{2.5}$ compositions.

## 2. METHODOLOGY

### 2.1 Model Configuration

Uncertainties are present in input data processing and in model execution. In addition, different capabilities embedded in models could produce large variations in simulated $PM_{2.5}$ concentrations (Yamaji *et al.*, 2020). Therefore, we used three different regional chemical transport models, namely the Community Multiscale Air Quality (CMAQ) modeling system (Byun and Schere, 2006) v. 5.2.1 and 5.0.2 (hereafter CMAQv5.2.1 and CMAQv5.0.2), and the Comprehensive Air Quality Model with Extensions (CAMx) (Ramboll Environ, 2016) v. 6.40, to evaluate the influences of uncertainties and different capabilities embedded in the three models. The SAPRC07 (Carter, 2010) chemical mechanism is common to all three models. The AERO6 and coarse/fine (CF) aerosol schemes were used in CMAQ and CAMx, respectively.

Figure 1 shows the target study domains, with d02 nested inside d01. These domains are commonly used in model comparisons in Japan's Study for Reference Air Quality Modeling (J-STREAM) project (Chatani *et al.*, 2018). The larger domain (d01) covers Asian countries with a 45 km × 45 km grid and provides boundary concentrations for d02. The boundary concentrations for d01 were derived from the chemical atmospheric general circulation model for the study of the atmospheric environment and radiative forcing (CHASER) (Sudo *et al.*, 2002). The nested domain (d02) covers most of Japan

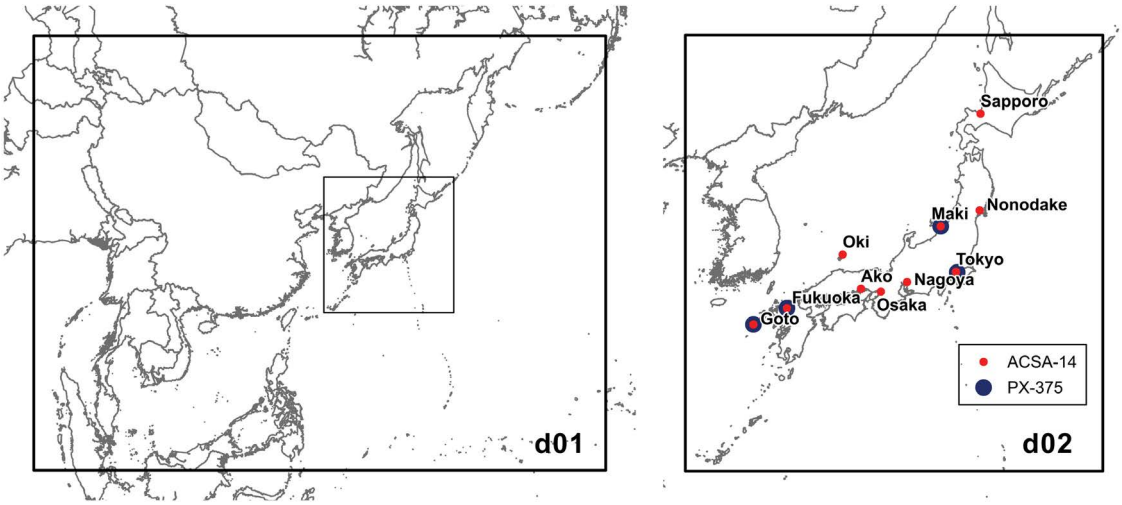


**Fig. 1.** Target domains (d02 nested inside d01) of the simulations performed in this study. The monitoring station sites are indicated by red and blue dots in d02.

with a 15 km × 15 km grid. Thirty layers were set vertically from the ground to 5,000 Pa. Hourly variations in meteorological fields and emissions were considered in the simulations. Details of the meteorological and emission inputs are described in Chatani *et al.* (2020a). Simulations were performed for the period from March 1, 2017, to March 31, 2018. The results for the first month were discarded as spin-up.

The base simulation, using all emission inputs, was performed using the three selected models. In addition, the source sensitivities of the simulated hourly $PM_{2.5}$ component concentrations were investigated. Three emission sources, namely volcanoes, dust, and anthropogenic sources in countries other than Japan (hereafter referred to as transboundary transport), were selected for this study. These isolated or distant sources are appropriate for investigating the drivers of change in hourly $PM_{2.5}$ component concentrations because their effects are apparent only when the airmass that was present at the distant source travels over the monitoring site. Source sensitivities were calculated using the Brute-Force Method (Chatani *et al.*, 2020a; Clappier *et al.*, 2017). The emissions of the target sources were subtracted entirely in the additional sensitivity simulations performed using CMAQv5.2.1. Differences in the simulated concentrations between the base and sensitivity simulations were evaluated as sensitivities to the corresponding sources.

## 2.2 Monitoring Data

In the continuous monitoring conducted by the MOEJ, the hourly concentrations of $PM_{2.5}$ components are continuously measured using two automatic instruments, a Continuous Dichotomous Aerosol Chemical Speciation Analyzer (ACSA-14; KIMOTO ELECTRIC Co., Ltd) and a Continuous Particulate Monitor with X-ray Fluorescence (PX-375; HORIBA Ltd.). ACSA-14 provides hourly mass concentrations of particulate matter (PM) and its components, including $H^+$, $SO_4^{2-}$, $NO_3^-$, and water-soluble organic compounds (WSOCs) in the fine and coarse fractions, and optically measured black carbon (OBC) in the fine fraction. $PM_{2.5}$ mass concentrations, equivalent to those used in the Federal Register Method (FRM), are also generated. ACSA-14 and its earlier versions have been used in studies conducted in China (Pan *et al.*, 2019; Ye *et al.*, 2019) and Japan (Itahashi *et al.*, 2017; Uno *et al.*, 2017a, b). ACSA-14 has been installed by MOEJ at ten locations in Japan (Fig. 1). PX-375 provides hourly mass concentrations of the metals in $PM_{2.5}$, including Ti, V, Cr, Mn, Fe, Ni, Cu, Zn, As, Pb, Al, Si, S, K, and Ca. PX-375 has been used in scientific studies conducted in China (Li *et al.*, 2017) and Japan (Asano *et al.*, 2017). PX-375 has been installed by the MOEJ at four locations in Japan (Fig. 1). Flags have been given to the data which needs careful treatments. The data containing measurement errors, maintenance, calibration, and contamination, as well as independent outliers, were excluded in this study.

It is important to note that the methods used to classify particles into fine and coarse fractions are not consistent between ACSA-14 and PX-375, which use a virtual imp-

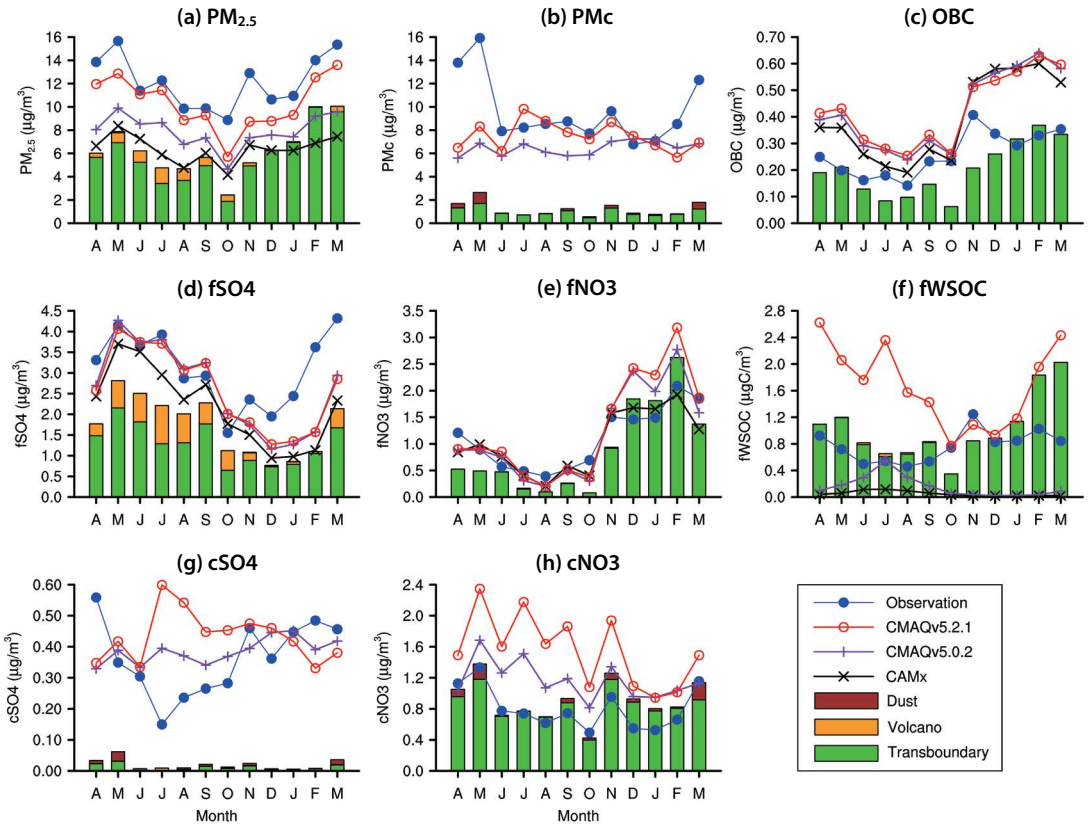


**Fig. 2.** Air quality parameters for the target domains in Japan, showing the observed and simulated monthly mean concentrations and source sensitivities. $PM_{2.5}$: ambient fine particulate matter < 2.5 μm. PMc: coarse-fraction PM. OBC, fSO4, fNO3, and fWSOC: fine-fraction contents of optically measured black carbon, $SO_4^{2-}$, $NO_3^-$, and water-soluble organic carbon. cSO4 and cNO3: coarse-fraction $SO_4^{2-}$ and $NO_3^-$. The values were averaged over all hours in each month at the ten stations using the ACSA-14. Concentrations are denoted by lines and markers; sensitivities by cumulative bars. Models used: CMAQ v. 5.2.1, CMAQ v. 5.0.2, and CAMx.

actor and a FRM impactor, respectively. Although both are intended to classify $PM_{2.5}$, Nakatsubo *et al.* (2018) reported differences between the $PM_{2.5}$ mass concentrations classified by ACSA-14 and FRM. Further, the methods used to represent particle size distributions are not consistent between CMAQ and CAMx. CMAQ uses three modal size distributions and $PM_{2.5}$ is represented by the Aitken and accumulation modes (Binkowski and Roselle, 2003). CAMx uses two discrete bins for coarse and fine particles, and the latter represents $PM_{2.5}$. These different treatments and particle evolution may result in differences in $PM_{2.5}$ concentrations simulated by them. It is difficult to maintain strict particle size consistency among the observed and simulated values. We compared the simulated values of the Aitken and accumulation modes of CMAQ and the "fine" bin of CAMx, with the observed PX-375 and ACSA-14 (fine fraction) values. CMAQ-simulated values of the coarse mode were compared with the observed ACSA-14 coarse-fraction values. Although using inconsistent size classifications might result in data gaps, our discussion focused mainly on the correlation between the observed and simulated concentrations.

## 3. RESULTS AND DISCUSSION

Figure 2 shows the observed and simulated monthly mean concentrations of $PM_{2.5}$, PM in the coarse fraction (PMc), OBC, $SO_4^{2-}$, $NO_3^-$, and WSOC in the fine fraction (OBC, fSO4, fNO3, and fWSOC, respectively), and $SO_4^{2-}$ and $NO_3^-$ in the coarse fraction (cSO4 and cNO3, respectively), along with the monthly mean source sensitivities simulated by CMAQv5.2.1. The values were averaged over all hours of each month at the ten ACSA-14 stations. The corresponding values at each ACSA-14 station are shown in Fig. S1 in the Supplementary Materials. The

simulated concentrations of elemental carbon (EC) were compared with the observed OBC concentrations. WSOC is a marker of secondary organic aerosols (SOAs) (Kondo *et al.*, 2007; Miyazaki *et al.*, 2006). The simulated concentrations of secondary organic carbon (SOC) were compared with the observed WSOC concentrations.

Distinct seasonal variations in $PM_{2.5}$ concentrations were observed (Fig. 2a), with higher concentrations in the spring and lower concentrations in the summer and early autumn. Although these seasonal variations were reproduced well by the models, the absolute values were underestimated. Among the three models, the CMAQv5.2.1-simulated values were the closest to the observed value. The underestimation was more evident in eastern Japan, as indicated by Chatani *et al.* (2020a). The $PM_{2.5}$ concentrations simulated by CMAQv5.2.1 were higher than the observed values at Fukuoka, which is located in western Japan (Fig. S1a). The simulated sensitivity to transboundary transport corresponded to 30–80% of the simulated $PM_{2.5}$ concentrations.

The models performed well in terms of simulating PMc concentrations, except in the spring, during which higher peaks were observed (Fig. 2b). The simulated sensitivities of PMc concentrations to volcanic emissions, dust, and transboundary transport were relatively small. The influence of other emission sources, including sea salt, seemed to be larger, given that Na and Cl were the most influential components in the simulated PMc concentrations (not shown).

The statistical model performances for the entire target period are presented in Table 1 including the annual mean observed and simulated concentrations, normalized mean bias (NMB), normalized mean error (NME), and correlation coefficients (Emery *et al.*, 2017). The NME and correlation coefficients were calculated from the daily and hourly concentrations (NMB is identical, by definition, whether calculated from the daily or hourly concentrations). The NME and correlation coefficients calculated from the daily $PM_{2.5}$ concentrations simulated by the three models satisfied the criteria proposed by Emery *et al.* (2017). However, using the hourly concentrations reduced the model performance. This indicates that it is

**Table 1.** Air quality model performances for the entire target period (April 1, 2017–March 31, 2018), based on annual mean observed (Obs.) and simulated (Sim.) concentrations in Japan.

| Species | Model | Obs. ($\mu g/m^3$) | Sim. ($\mu g/m^3$) | NMB (%) | Daily | | Hourly | |
|---|---|---|---|---|---|---|---|---|
| | | | | | NME (%) | *R* | NME (%) | *R* |
| $PM_{2.5}$ | CMAQv5.2.1 | 12.1 | 10.3 | −14.8 | 36.4 | 0.76 | 45.9 | 0.67 |
| | CMAQv5.0.2 | 12.1 | 7.94 | −34.7 | 40.3 | 0.76 | 47.0 | 0.66 |
| | CAMx | 12.1 | 6.41 | −47.2 | 49.2 | 0.75 | 53.8 | 0.65 |
| PMc | CMAQv5.2.1 | 9.45 | 7.36 | −22.0 | 48.1 | 0.50 | 59.6 | 0.42 |
| | CMAQv5.0.2 | 9.45 | 6.42 | −32.1 | 56.7 | 0.30 | 66.1 | 0.24 |
| OBC | CMAQv5.2.1 | 0.26 | 0.43 | 63.0 | 85.3 | 0.67 | 103.7 | 0.55 |
| | CMAQv5.0.2 | 0.26 | 0.42 | 60.8 | 84.5 | 0.66 | 103.0 | 0.55 |
| | CAMx | 0.26 | 0.40 | 50.0 | 79.1 | 0.69 | 98.7 | 0.56 |
| fSO4 | CMAQv5.2.1 | 3.08 | 2.61 | −15.2 | 43.4 | 0.73 | 55.8 | 0.64 |
| | CMAQv5.0.2 | 3.08 | 2.64 | −14.4 | 43.7 | 0.73 | 56.3 | 0.64 |
| | CAMx | 3.08 | 2.19 | −28.9 | 48.5 | 0.69 | 58.6 | 0.61 |
| fNO3 | CMAQv5.2.1 | 1.10 | 1.29 | 17.4 | 80.3 | 0.62 | 101.6 | 0.50 |
| | CMAQv5.0.2 | 1.10 | 1.17 | 6.66 | 77.9 | 0.57 | 99.0 | 0.46 |
| | CAMx | 1.10 | 1.02 | −6.85 | 74.0 | 0.55 | 97.6 | 0.41 |
| fWSOC | CMAQv5.2.1 | 0.76 | 1.67 | 119.7 | 148.8 | 0.39 | 160.9 | 0.37 |
| | CMAQv5.0.2 | 0.76 | 0.16 | −79.4 | 86.5 | 0.01 | 88.2 | 0.04 |
| | CAMx | 0.76 | 0.05 | −93.2 | 93.4 | −0.08 | 93.7 | −0.03 |
| cSO4 | CMAQv5.2.1 | 0.36 | 0.43 | 20.3 | 115.2 | 0.20 | 160.6 | 0.09 |
| | CMAQv5.0.2 | 0.36 | 0.39 | 8.30 | 113.5 | 0.15 | 158.0 | 0.07 |
| cNO3 | CMAQv5.2.1 | 0.80 | 1.55 | 93.4 | 106.3 | 0.70 | 121.4 | 0.58 |
| | CMAQv5.0.2 | 0.80 | 1.16 | 44.9 | 72.2 | 0.64 | 89.3 | 0.53 |

NMB: normalized mean bias; NME: normalized mean error; *R*: correlation coefficient. NME and *R* are based on daily and hourly concentrations. $PM_{2.5}$: ambient fine particulate matter < 2.5 μm. PMc: coarse-fraction PM. OBC, fSO4, fNO3, and fWSOC: fine-fraction optically measured black carbon, $SO_4^{2-}$, $NO_3^-$, and water-soluble organic carbon. cSO4 and cNO3: coarse-fraction $SO_4^{2-}$ and $NO_3^-$.

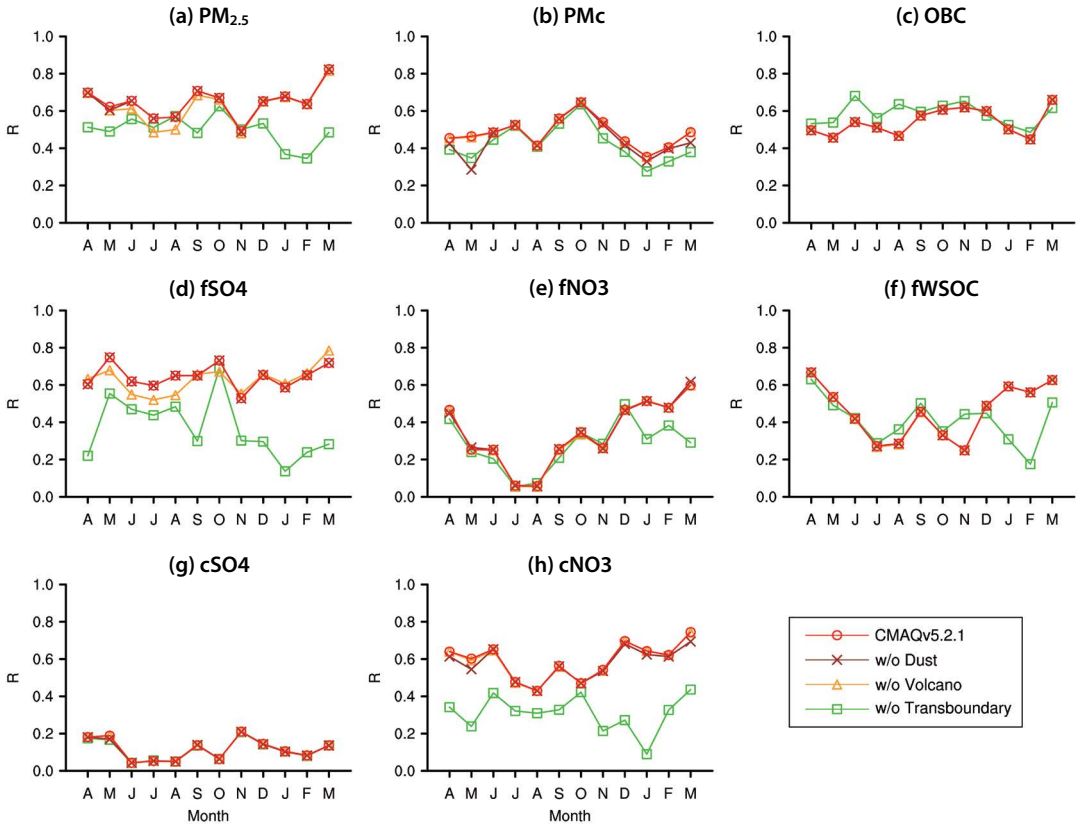


**Fig. 3.** Monthly variations in correlation coefficients of air quality parameters for the target domains in Japan, based on hourly concentrations of particulate matter (PM) and its components at all ten ACSA-14 stations. CMAQv5.2.1: values simulated using CMAQ v. 5.2.1 in the base and sensitivity simulations. $PM_{2.5}$: ambient fine PM < 2.5 μm. PMc: coarse-fraction PM. OBC, fSO4, fNO3, and fWSOC: fine-fraction optically measured black carbon, $SO_4^{2-}$, $NO_3^-$, and water-soluble organic carbon. cSO4 and cNO3: coarse-fraction $SO_4^{2-}$ and $NO_3^-$. w/o: without.

more challenging for models to reproduce hourly concentrations of PM and its components.

Figure 3 shows monthly variations in the correlation coefficients calculated from the hourly concentrations of PM and its components at all ten ACSA-14 stations, derived from the CMAQv5.2.1 base and sensitivity simulations. The corresponding values at each ACSA-14 station are shown in Fig. S2 in the Supplementary Materials. The correlation coefficients of $PM_{2.5}$ and PMc were higher in the base simulation than in the sensitivity simulations (Fig. 3a, b). This implies that volcanic emissions, dust emissions, and transboundary transport improved the correlation between the observed and simulated hourly $PM_{2.5}$ and PMc concentrations.

The model performances and source sensitivities of $PM_{2.5}$ and PMc reflected those of their components. These are discussed in detail in the following subsections.

### 3.1 OBC

OBC concentrations were overestimated by the three models throughout the target period (Fig. 2c). Sensitivity to transboundary transport corresponded to 24–58% of the simulated OBC concentrations. It must be noted that the OBC concentrations obtained by ACSA-14 tend to be lower than the EC concentrations. Nakatsubo *et al.* (2018) reported that OBC concentrations obtained by ACSA-14 were approximately 40% lower than EC concentrations in their comparison. Therefore, the absolute magnitude of the overestimation in this study may have been affected by the performance of ACSA-14 for OBC. Regardless, the base simulation yielded lower correlation coefficients than the sensitivity simulation without transboundary transport (Fig. 3c). Including transboundary transport reduced the correlation between the observed and simulated OBC concentrations. In contrast, lower correlation coefficients in the base simulation are not evident at each

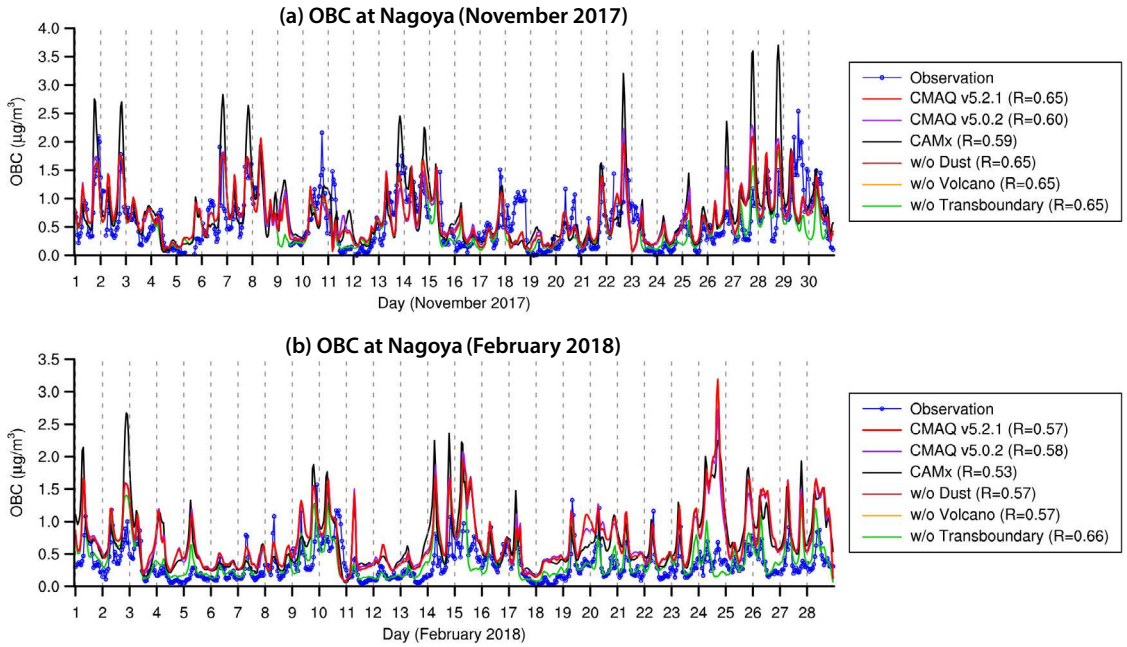


**Fig. 4.** Observed and simulated hourly fine-fraction optically measured black carbon (OBC) at Nagoya, Japan, in (a) November 2017 and (b) February 2018. Simulated values are based on the three models used for the base and sensitivity simulations. Models used: CMAQ v. 5.2.1, CMAQ v. 5.0.2, and CAMx. w/o: without.

station(Fig. S2c). Thus, the inclusion of transboundary transport reduced the spatial correlations among the ten ACSA-14 stations, whereas it contributed to better temporal correlations, particularly at stations located in remote areas of western Japan such as Oki and Goto. As shown in Fig. S1c, the base simulation had a better performance at the stations located in urban areas, including Sapporo, Tokyo, Nagoya, and Osaka. Overestimation mainly occurred in remote areas when influences of transboundary transport were large. The inclusion of transboundary transport resulted in spatial inconsistencies in model performance between urban and remote areas.

Figure 4 compares the observed hourly OBC concentrations with the simulated concentrations generated by the base (three models) and sensitivity simulations; as an example, the results in November 2017 and February 2018 are shown for Nagoya. The absolute values and hourly variations observed in November 2017 were reproduced well by the three models (Fig. 4a). Based on hourly concentrations, OBC peaked mainly in the evenings when atmospheric conditions are relatively stable. CAMx simulated higher OBC concentrations than CMAQ at peak hours. Chatani *et al.* (2014) indicated that simulated EC (OBC) concentrations were greatly affected by the treatment of vertical diffusion. Although both CMAQ and CAMx use the Asymmetric Convective Model v. 2 (ACM2) vertical diffusion scheme (Pleim, 2007), CMAQ forces vertical diffusion coefficients to be greater than 1.0 $m^2/s$ in urban areas, including Nagoya. The higher OBC concentrations simulated by CAMx were likely caused by the different lower limits of the vertical diffusion coefficients in urban areas under the stable atmosphere. To improve the model performance for OBC concentrations at peak hours, it is necessary to improve the treatment of vertical diffusion.

Throughout February 2018, the simulated OBC concentrations were slightly higher than the observed values (Fig. 4b). There were distinct gaps between the OBC concentrations obtained in the base simulation and the sensitivity simulation without transboundary transport, indicating that transboundary transport caused the overestimation, as well as a poorer correlation. This was particularly evident in the peak on February 24. The results suggest that BC emissions in countries other than Japan have been overestimated.

Kanaya *et al.* (2020) indicated that their simulation tended to overestimate the BC concentrations at Fukue Island, located between Japan and the continent, when the airmass was transported from China and South Korea. Choi *et al.* (2020) implied that the existing emission

inventories, including the Hemispheric Transport of Air Pollution (HTAP) emissions v. 2.2 (Janssens-Maenhout *et al.*, 2015), used in this study, overestimated the BC/CO ratios of the emissions in China and South Korea. The results obtained in this study were consistent with their findings. However, it must also be noted that February 2018, which had larger discrepancies between the observed and simulated OBC concentrations (Fig. 2c), had the lowest correlation coefficients (0.48), even in the sensitivity simulation without transboundary transport (Fig. 3c). Both the decrease in OBC originating from transboundary transport and the increase in OBC originating from local emissions are expected to improve spatial correlations.

### 3.2 $SO_4^{2-}$

The statistical model performance for fSO4 was comparable to that for $PM_{2.5}$ (Table 1), satisfying the criteria proposed by Emery *et al.* (2017). The observed fSO4 concentrations were higher during the first half of the target period (spring and summer; Fig. 2d). Their absolute values and monthly variations were reproduced well by the three models. In contrast, during the second half of the target period (autumn and winter), these values were underestimated by the three models. Previous studies (Itahashi *et al.*, 2018b; Morino *et al.*, 2015) also reported the underestimation of winter $SO_4^{2-}$ concentrations around Japan. The models may need to be updated by including additional aqueous- and gaseous-phase oxidation pathways, to improve their performances for winter $SO_4^{2-}$ values (Itahashi *et al.*, 2019, 2018a). Itahashi *et al.* (2018b) indicated that differences between CAMx and CMAQv5.0.2 regarding how dry deposition is represented resulted in CAMx simulating higher $SO_4^{2-}$ concentrations. The opposite pattern that we obtained in this study may be due to another difference: we used CMAQ v5.0.2 calculating photolysis rates online, whereas CAMx picked them up from a lookup table. Differences in photolysis rates could affect the secondary formation of relevant species in the atmosphere, including $SO_4^{2-}$ (Chatani *et al.*, 2020b; Itahashi *et al.*, 2020b).

For fSO4, the simulated concentration sensitivities to transboundary transport and volcanic emissions were notable, at 32–67% and 2–25% of the simulated concentrations, respectively (Fig. 2d). Throughout the target period, the correlation coefficients in the sensitivity simulation without transboundary transport were notably lower than those in the base simulation (Fig. 3d). This clearly reflects the contribution of transboundary transport to improving the correlation between the observed

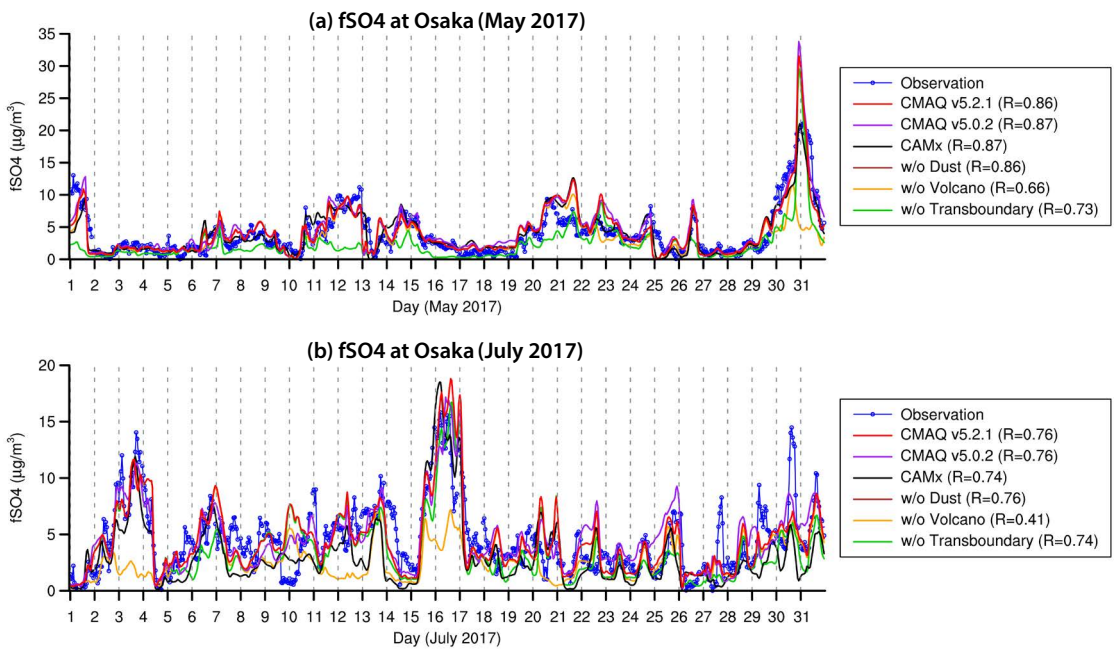


**Fig. 5.** Observed and simulated hourly fine-fraction $SO_4^{2-}$ (fSO4) concentrations at Osaka, Japan, in (a) May 2017 and (b) July 2017. Simulated values are based on the three models used in the base and sensitivity simulations. Models used: CMAQ v. 5.2.1, CMAQ v. 5.0.2, and CAMx. w/o: without.

and simulated fSO4 concentrations. The contribution of volcanic emissions was also evident from May to August.

Figure 5 compares the observed hourly fSO4 concentrations with the simulated concentrations derived from the base (three models) and sensitivity simulations, using Osaka in May and July 2017 as an example. Hourly variations in observed fSO4 concentrations were reproduced well by the three models. The fSO4 concentrations simulated in the sensitivity simulation without transboundary transport had distinctly lower peaks than those simulated in the base simulation on May 1, 12, 20, and 30 (Fig. 5a), clearly illustrating the influence of transboundary transport on these days. Likewise, the fSO4 concentrations simulated in the sensitivity simulation without volcanic emissions had distinctly lower peaks on July 3, 12, and 16 (Fig. 5b), clearly illustrating influence of volcanic emissions on these days.

In contrast, the models performed worse in simulating cSO4 concentrations (Table 1). While the observed and simulated annual cSO4 concentrations were comparable, the NME was large and the correlation coefficients were quite low (Fig. 3g). The simulated sensitivities of cSO4 concentrations to the three emission sources were small (Fig. 2g). This implies that the factors affecting cSO4 were entirely different from those affecting fSO4. Osada *et al.* (2016) reported low correlations between cSO4 concentrations measured using the ACSA and those measured by collection on filters. These findings suggest that there are large uncertainties in both the observed and simulated cSO4 concentrations.

### 3.3 $NO_3^-$

There were distinct seasonal variations in the fNO3 concentration (Fig. 2e). Observed fNO3 concentrations were much higher during the winter than the summer. This seasonal variation was reproduced well by the models. However, the higher winter fNO3 concentrations were overestimated by the CMAQ models, particularly in western Japan, including Oki, Goto, and Fukuoka (Fig. S1e). Most of the overestimation was due to transboundary transport, even though it improved the correlation during the winter (Fig. 3e and Fig. S2e). The overestimation of summer $NO_3^-$ concentrations, which has been previously reported (Shimadera *et al.*, 2014), was not evident in this study. The observed cNO3 concentrations did not exhibit distinct seasonal variations (Fig. 2h). In contrast to fNO3, the models overestimated cNO3 throughout the target period. Transboundary transport improved the cNO3 correlations (Fig. 3h).

Figure 6 compares the observed hourly fNO3 concentrations with the simulated concentrations derived from the base (three models) and sensitivity simulations, using February 2018 in Tokyo (eastern Japan) and Fukuoka (western Japan), as examples. At Tokyo, while the observed fNO3 concentrations were relatively low on most days, there were peaks on some days (Fig. 6a). The models did not satisfactorily reproduce some of these peaks (those on February 3 and 11). Itahashi *et al.* (2020b) conducted a detailed analysis of the model performance for winter $NO_3^-$ concentrations in Tokyo, finding that $NO_X$ and $NH_3$ emissions, heterogeneous reactions involving HONO, and photolysis rates were critical factors that affect model performance in terms of simulating $NO_3^-$ concentration peaks. Unlike Tokyo, at Fukuoka (western Japan) many of the peaks were higher, albeit flatter, and all were significantly overestimated by the CMAQ models (Fig. 6b). The fNO3 concentrations and correlation coefficients based on the sensitivity simulation without transboundary transport were substantially lower than those in the base simulation, indicating that they were exclusively and excessively affected by transboundary transport. Uno *et al.* (2020) indicated that the recent reduction in $SO_X$ emissions realized by the stringent emission controls implemented in China caused a paradigm shift and increased $NO_3^-$ transport to western Japan, particularly during colder seasons (Itahashi *et al.*, 2017). Although their findings are related to our simulated results, the influence of transboundary transport on the fNO3 concentration was too large. As mentioned, the winter fSO4 concentrations were underestimated by the models used in this study. When more fSO4 is available, the simulated fNO3 concentrations should decrease, according to the paradigm discussed by Uno *et al.* (2020). The possible impacts of improved model performance on winter fSO4 concentrations (discussed in section 3.2), are also important for addressing the problem of overestimated fNO3 concentrations. Further, the CAMx-simulated peak values were substantially lower than those simulated by CMAQ. It is known that the inaccurate estimation of gaseous $HNO_3$ dry deposition velocity can cause the overestimation of $NO_3^-$ concentrations (Itahashi *et al.*, 2017; Morino *et al.*, 2015; Shimadera *et al.*, 2014). CMAQ and CAMx use different dry deposition schemes, M3DRY (Otte and Pleim, 2010) and that of Zhang *et al.* (2003), respectively, which might have caused the differences in the fNO3 concentrations simulated by CMAQ and CAMx. More

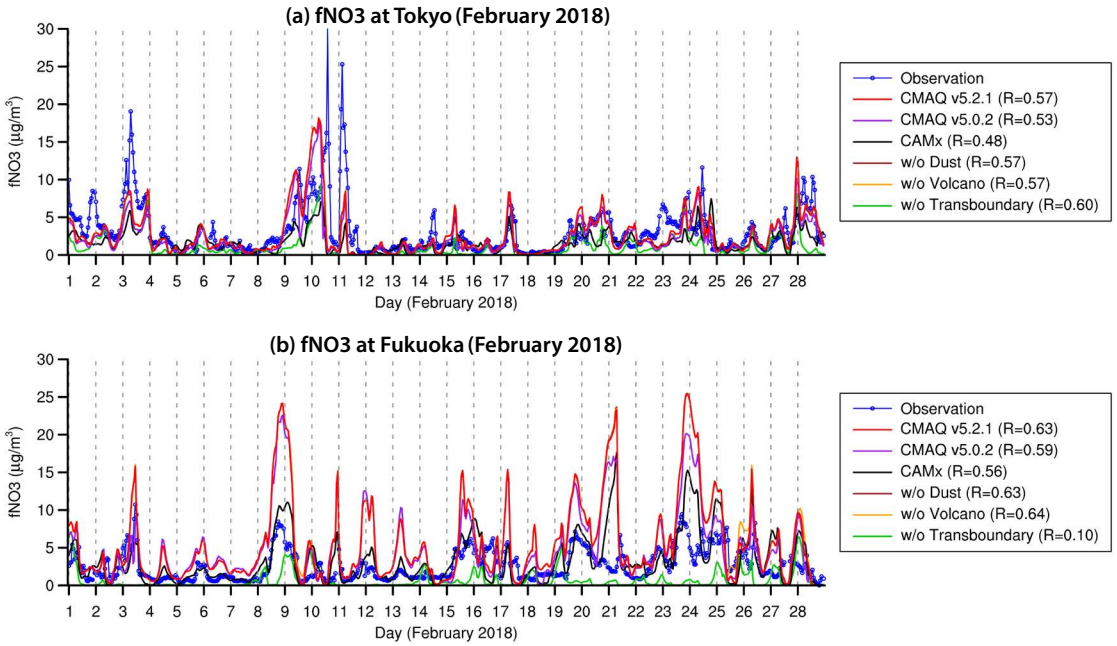


**Fig. 6.** Observed and simulated hourly fine-fraction $NO_3^-$ (fNO3) concentrations in February 2018 at (a) Tokyo and (b) Fukuoka. Simulated values are based on the three models used in the base and sensitivity simulations. Models used: CMAQ v. 5.2.1, CMAQ v. 5.0.2, and CAMx. w/o: without.

accurate methods of representing the dry deposition of gaseous $HNO_3$ are therefore required.

Figure 7a compares the observed hourly fNO3 concentrations and the simulated hourly concentrations derived from the base (three models) and sensitivity simulations, for Tokyo in July 2017, when the fNO3 concentrations and their correlation were remarkably low (Figs. 2e and 3e). Figure 7b shows the observed and simulated hourly cNO3 concentrations, and Figure 7c shows the cumulative concentrations of cNO3, fNO3, and stoichiometrically equivalent gaseous $HNO_3$, simulated by CMAQ v5.2.1, along with temperatures and relative humidities in the corresponding month and location. The observed fNO3 concentrations were mostly below 1 μg/m$^3$. There were peaks in the simulated fNO3 values on some days. These overestimated peaks greatly reduced the correlation between the observed and simulated fNO3 concentrations. Although the observed and simulated cNO3 concentrations were higher at the corresponding hours, their variations were smaller than those of fNO3, and were reproduced relatively well by the models.

The simulated gaseous $HNO_3$ concentrations were higher during the daytime due to photochemical formation induced by solar radiation (Fig. 7c). However, the ISORROPIA phase equilibrium model (Fountoukis and Nenes, 2007) embedded in CMAQ and CAMx did not partition the gaseous $HNO_3$ into fNO3 and cNO3 because of the higher daytime temperature and lower relative humidity. The simulated fNO3 peaks occured mostly in the early morning, when the temperature was low and humidity was high, and when ample gaseous $HNO_3$ remained. The strong dependency of the simulated partitioning of $NH_4NO_3$, a major component of fNO3, on temperature and humidity, as well as on the concentrations of the associated species, causes instability and rapid variations in the simulated fNO3 concentrations (Nenes *et al.*, 2020). It is challenging for models to reproduce hourly variations in all of the related factors. Moreover, it is necessary to validate hourly variations of gaseous $HNO_3$ to check if the simulated dynamic behaviors surely occur in the real atmosphere.

However, the cNO3 concentrations were appropriately simulated. In the coarse fraction, $NO_3^-$ appears to be present in more stable forms, including as $NaNO_3$ (Kajino *et al.*, 2013; Dasgupta *et al.*, 2007). Further, the dynamic mass transfer considered in the models requires a longer time for the coarse fraction particles to reach equilibrium (Kelly *et al.*, 2010). These factors may have resulted in smaller variations and and overall better model performance regarding cNO3 concentrations.

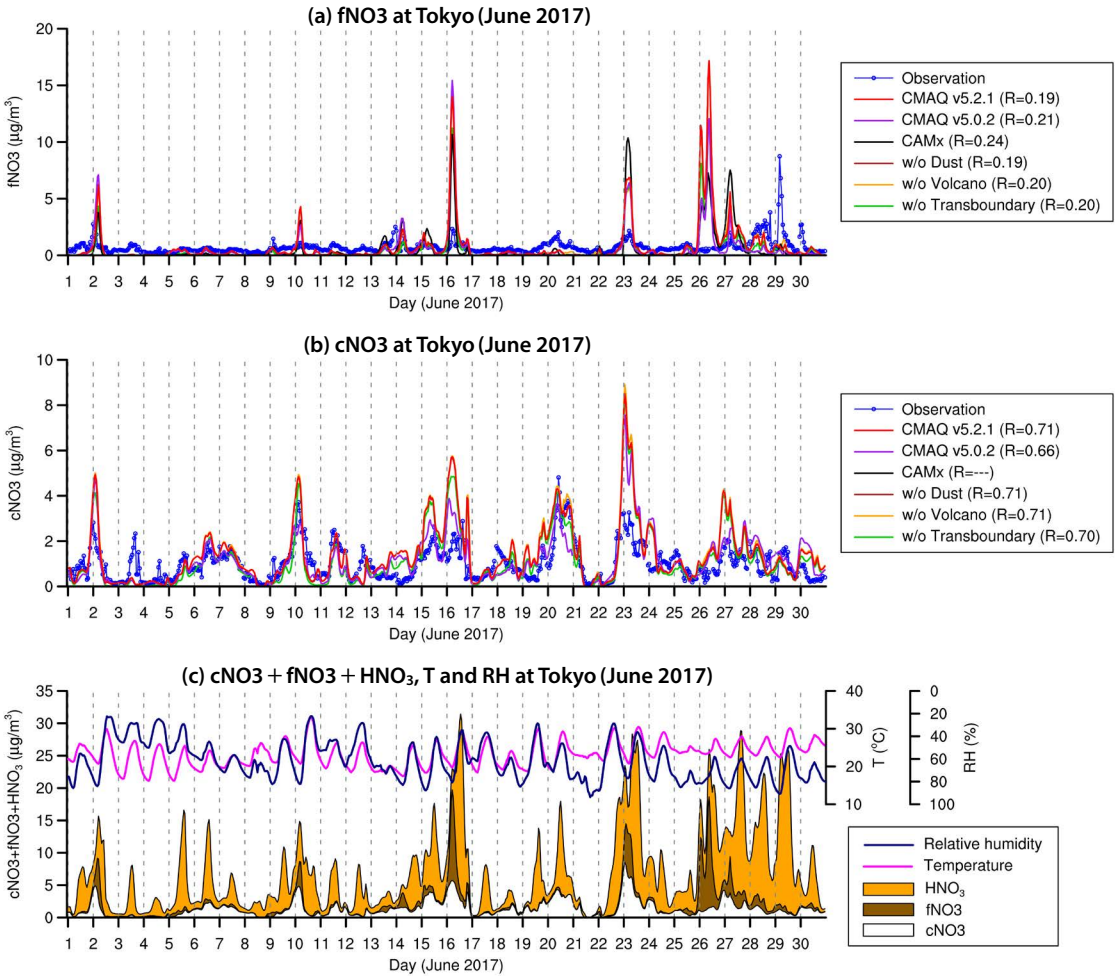


**Fig. 7.** Observed and simulated hourly concentrations of (a) fine-fraction and (b) coarse-fraction $NO_3^-$ (fNO3 and cNO3, respectively), based on the three models used in the base and sensitivity simulations, for Tokyo in June 2017. (c) Cumulative hourly concentrations of cNO3, fNO3, gaseous $HNO_3$ (simulated by CMAQ v. 5.2.1), temperature, and relative humidity, in the base and sensitivity simulations. Models used: CMAQ v. 5.2.1, CMAQ v. 5.0.2, and CAMx. w/o: without.

### 3.4 WSOC

As SOAs form via photochemical reactions, the SOC concentrations simulated by CMAQv5.0.2 and CAMx were high during July (Fig. 2f) when photochemical reactions are active. Although the July SOC concentrations simulated by CMAQv5.0.2 were comparable to the observed fWSOC concentrations, those in other months were significantly underestimated by the model. The SOA concentrations simulated by CMAQv5.2.1 were much higher than the observed fWSOC concentrations and the SOC concentrations simulated by CMAQv5.0.2 and CAMx in the corresponding months. The increase in SOC concentrations from December to March simulated by CMAQv5.2.1 was greatly affected by transboundary transport, which contributed to a better correlation between the observed and simulated values (Fig. 3f). The contribution of transboundary transport was smaller during the spring and summer.

The observed fWSOC concentrations were lower in summer, implying that their seasonal variations cannot be explained simply by the strength of photochemical reactions. Another potential factor is biomass burning emissions, which also contribute to WSOC (Ikemori *et al.*, 2021; Yan *et al.*, 2015). However, the absolute magnitude and seasonal variations of the observed WSOC concentrations require careful attention. Saito *et al.* (2020) compared the fWSOC concentrations measured by ACSA-14 and the conventional method. They found seasonal varia-

tions in the slopes and intercepts of the regression lines between them. The discrepancies were larger in the summer than the winter, possibly caused by seasonal variations in the WSOC compositions. In addition, components including levoglucosan, which is a well known marker for biomass burning emissions, cannot be detected by ACSA-14 using ultraviolet spectrophotometry. Additional research is necessary to clarify the relationships among fWSOC concentrations measured by ACSA-14 and by the conventional method, as well as SOA concentrations simulated by the models.

CMAQ v. 5.2 and later versions have incorporated partitioning and aging of semi-volatile organic aerosols (Robinson *et al.*, 2007; Donahue *et al.*, 2006). Along with this treatment, they have introduced a new surrogate species, which is a potential SOA from combustion emissions (pcSOA). pcSOA represents the SOA that was missed in the preceding models for various reasons, including SOA formation from intermediate-volatility organic compound (IVOC) emissions, which are not included in current emission inventories (Murphy *et al.*, 2017). In CMAQv5.2.1, an amount equivalent to 6.6 times the primary organic aerosol (POA) emissions is ingested as missing emissions of pcVOC (precursors of pcSOA), which are subsequently oxidized in the atmosphere to form pcSOA. In our simulations, pcSOA occupied a large fraction of the simulated SOC concentrations (not shown), leading to overestimation and differences in seasonal variations of the simulated SOC concentrations (Fig. 2f).

Figure 8 compares the observed hourly fWSOC concentrations with the simulated SOC concentrations derived from the base (three models) and sensitivity simulations, using Tokyo in March 2018 and July 2017 as an example. The SOA concentrations simulated by CMAQ v5.2.1 significantly overestimated the broad increases in the fWSOC concentrations on March 11–15 and 25–31 (Fig. 8a). For the same periods, the SOA concentrations simulated in the sensitivity simulation without transboundary transport were much lower, indicating that the overestimation was caused mainly by transboundary transport. It is worth noting that the correlation coefficient in the base simulation (0.79) was higher than that in the sensitivity simulation without transboundary transport (0.67). Part of the increase in observed fWSOC concentrations likely reflects SOA formed from IVOC emissions in upwind countries. In contrast, the SOC concentrations simulated in the base and sensitivity simulations without transboundary transport were similar; both simulations overestimated the increases on July 7–9

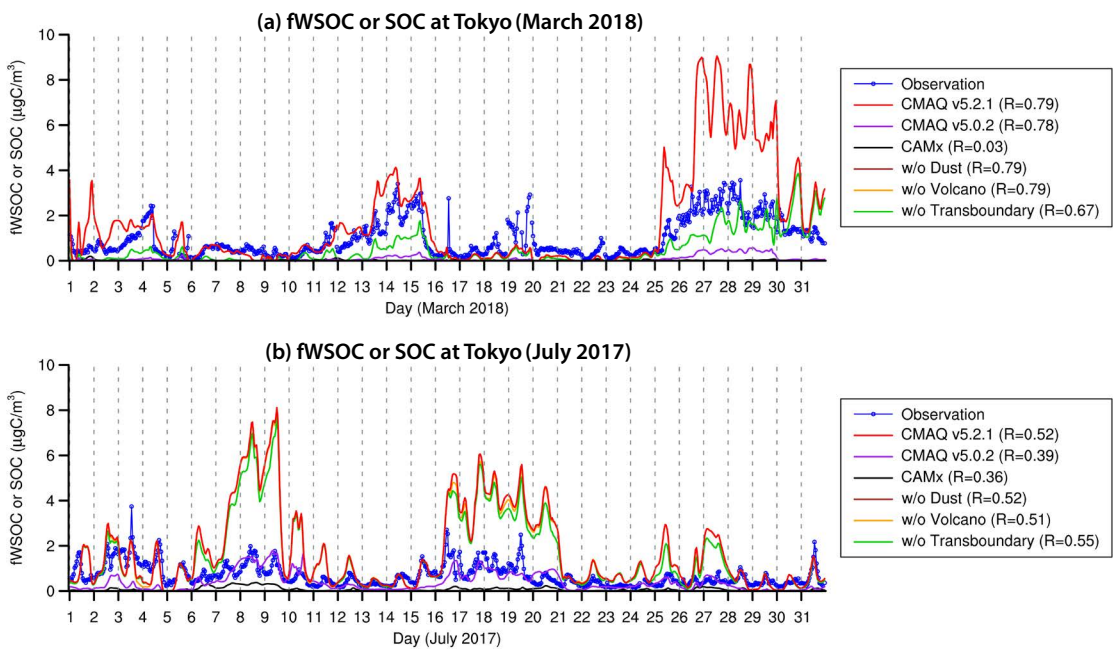


**Fig. 8.** Observed fine-fraction water-soluble organic compound (fWSOC) and simulated hourly secondary organic carbon (SOC) concentrations, derived from the base and sensitivity simulations for Tokyo in (a) March 2018 and (b) July 2017. Models used: CMAQ v. 5.2.1, CMAQ v. 5.0.2, and CAMx. w/o: without.

and 16–20 (Fig. 8b). The SOC concentrations simulated by CMAQv5.0.2 were closer to the observed values in the corresponding period. The later versions of CMAQ did not perform well for modeling summer pcSOA formed from IVOC emissions in Japan.

The emission ratio of pcVOC to POA is an uncertain parameter in the treatment incorporated in CMAQv5.2.1 (Murphy *et al.*, 2017). While its value (6.6) has been validated in comparisons with observations conducted in the United States, this value may not be suitable for Asia, where POA emissions are relatively high because there are fewer emission controls. Suitable values for the pcVOC/POA ratio need to be examined based on the current conditions in Asia (Cai *et al.*, 2019; Morino *et al.*, 2018; Liu *et al.*, 2017). In addition, it may not be appropriate to apply a single pcVOC/POA ratio value to emissions from all sources, including biomass burning (Murphy *et al.*, 2017). However, in CMAQv5.2.1, only a single pcVOC/POA ratio can be used, because the model accepts only one emission input involving all emission sources. The subsequent CMAQ version (v. 5.3) has realized the incorporation of multiple emission inputs and their respective pcVOC/POA ratios.

### 3.5 Metals

Figure 9 shows the observed and simulated monthly mean concentrations of Ti, Mn, Fe, Al, Si, K, and Ca in the fine fraction, and the monthly mean source sensitivities simulated by CMAQv5.2.1, averaged over all hours in each month at four PX-375 stations. The corresponding values at each PX-375 station are shown in Fig. S3 in the Supplementary Materials. Figure 10 shows the monthly variations in the correlation coefficients calculated from the hourly metal concentrations at all the four PX-375 stations, derived from the CMAQv5.2.1 base and sensitivity simulations. The corresponding values at each PX-375 station are shown in Fig. S4 in the Supplementary Materials.

The model performance differed depending on the metal. While the concentrations of Mn, Fe, Al, and Si

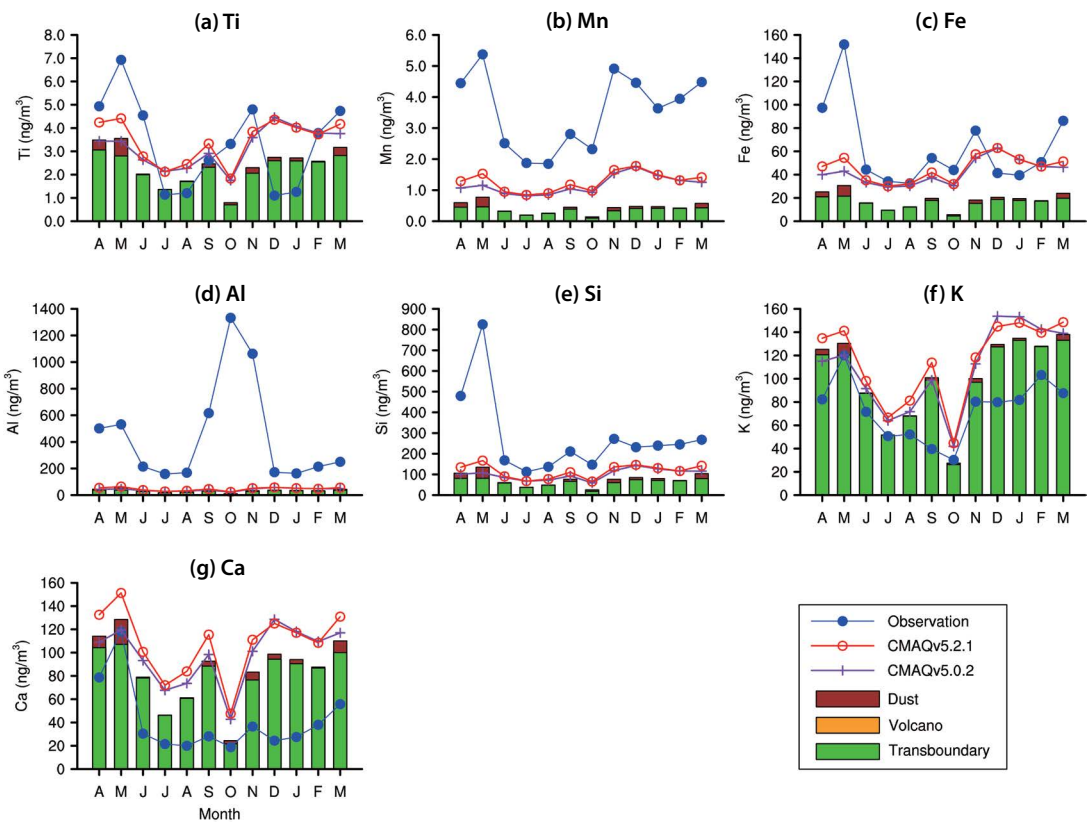


**Fig. 9.** Observed and simulated monthly mean concentrations and source sensitivities of Ti, Mn, Fe, Al, Si, K, and Ca in the fine fraction. Values were averaged over all hours in each month for the four stations. Measurements were performed using PX-375. Concentrations are denoted by lines and markers, sensitivities by cumulative bars. Models used: CMAQ v. 5.2.1 and CMAQ v. 5.0.2.

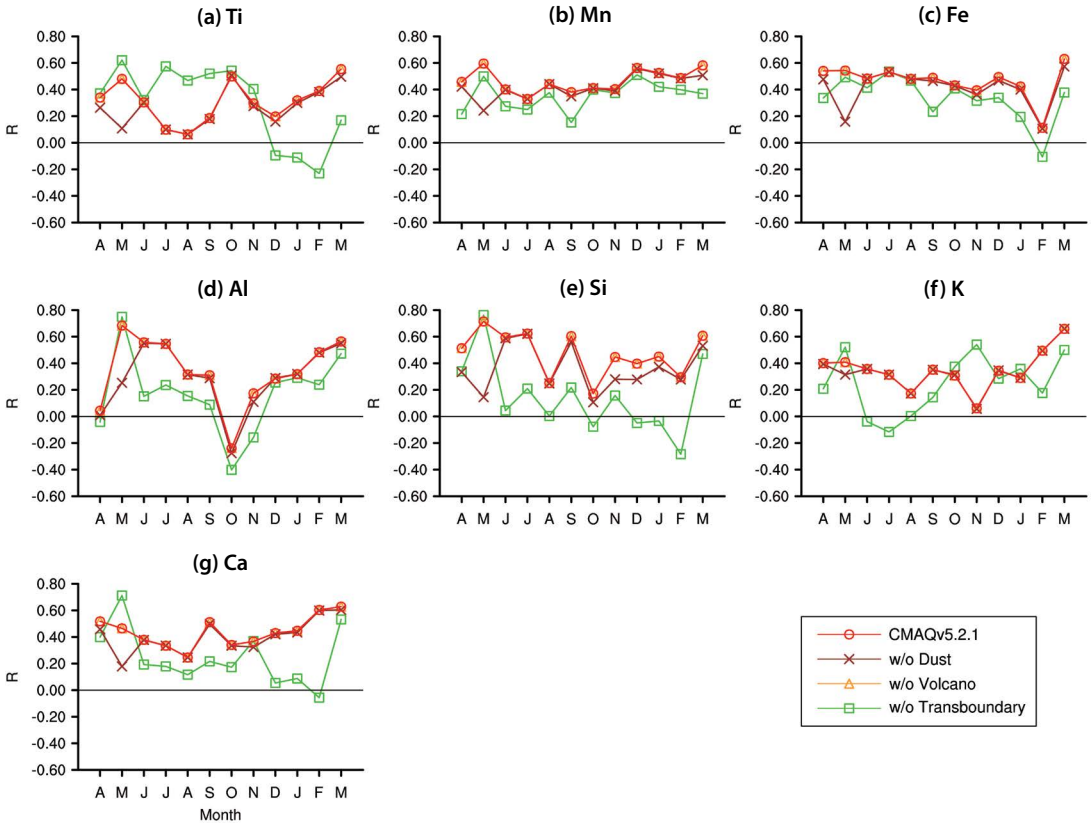


**Fig. 10.** Monthly variations in the correlation coefficients based on hourly metal concentrations (Ti, Mn, Fe, Al, Si, K, and Ca) in the fine fraction at all four PX-375 stations derived from the base and sensitivity CMAQ v. 5.2.1 simulations.

were all underestimated, K and Ca concentrations were overestimated. The influence of transboundary transport was apparent for all metals. The correlation coefficients of the base simulation were distinctly higher than those of the sensitivity simulation without transboundary transport. Transboundary transport contributed significantly to the simulated metal concentrations and improved the correlations. Itahashi *et al.* (2018a) described the importance of Mn and Fe in $SO_4^{2-}$ formation; therefore, PM speciation profiles that include Mn and Fe, as proposed by Fu *et al.* (2013), have been used for countries other than Japan. Although Fu *et al.* (2013) established profiles for 24 emission sectors, these sector profiles need to be merged into the four sectors that are available in the HTAP emissions used in this study. Differences in the profiles for different countries, regions within countries, and particular sectors with regions, were not considered. In this study, the rough treatment of the metal profiles in the PM may have reduced the model performance for metals. To address this problem, a detailed database of metal emissions is required for Japan and other countries (Kajino *et al.*, 2020).

The similarity of the physical processes embedded in CMAQv5.2.1 and CMAQv5.0.2 resulted in similar simulated metal concentrations. However, the metal concentrations simulated by CMAQv5.2.1 for May were much higher than those simulated by CMAQv5.0.2. CMAQ v5.2.1 implements the windblown dust emission parameterization of Foroutan *et al.* (2017), whereas dust emissions are not considered by CMAQv5.0.2 used in this study. Differences in the simulated metal concentrations were caused by dust emissions, as indicated by the simulated sensitivity toward them (Fig. 9), and by better correlations in the base simulation than the sensitivity simulation without dust emissions (Fig. 10).

Figure 11 compares the observed hourly Fe and Ca concentrations with the simulated concentrations derived from the CMAQv5.2.1 and CMAQv5.0.2 base and sensitivity simulations, using Fukuoka in May 2017 as an example. A heavy dust storm in east Asia at the beginning

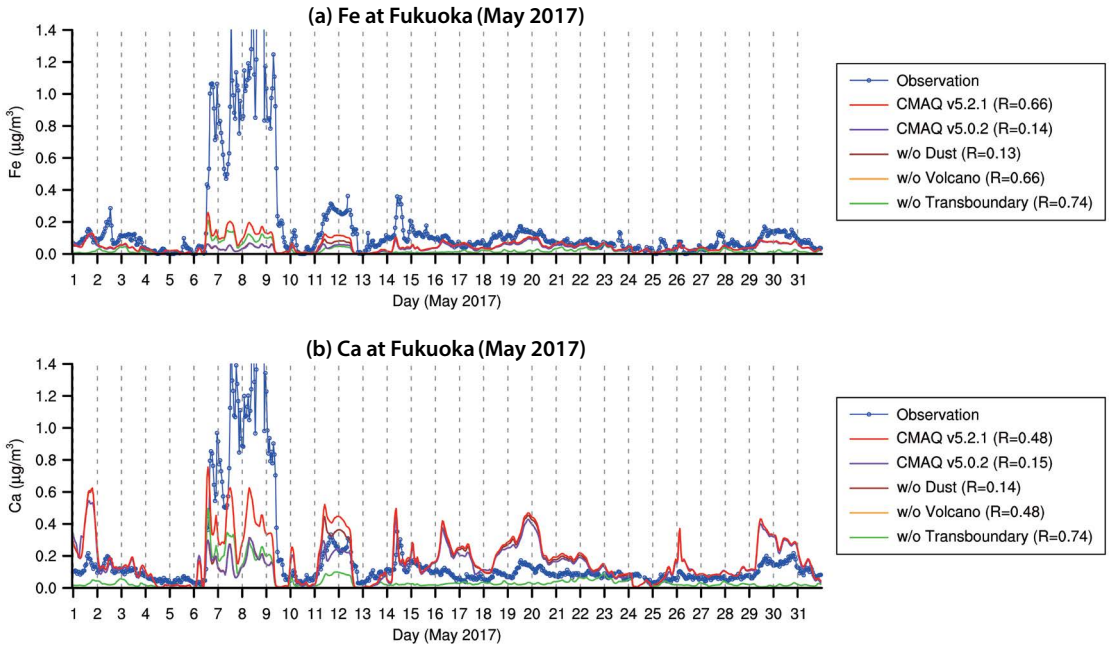


**Fig. 11.** Observed and simulated hourly concentrations of (a) Fe and (b) Ca, based on CMAQ v. 5.2.1 and CMAQ v. 5.0.2 base and sensitivity simulations, for Fukuoka in May 2017. w/o: without.

of May 2017 (Zhang *et al.*, 2018) caused distinct peaks in Fe and Ca concentrations on May 6–9. Although these peaks were not fully reproduced, the Ca concentrations from the base simulation were clearly higher than those from the sensitivity simulation without dust emissions. For Fe, the differences between the base and sensitivity simulations were marginal, although visible. The parameterization embedded in CMAQv5.2.1 satisfactorily reproduced some of the Fe and Ca peaks that originated from dust emissions. The peaks in Ca concentrations were overestimated after the dust storm. They were exclusively affected by transboundary transport, as indicated by the significantly low concentrations obtained in the sensitivity simulation without transboundary transport. Improved metal emissions and speciation profiles in other countries are required to improve the model performance.

## 4. CONCLUSIONS

This study evaluated the advantages of the continuous monitoring of $PM_{2.5}$ composition conducted by MOEJ for regional air quality simulations. Continuous monitoring contributed greatly in two respects: in identifying drivers of hourly variations in $PM_{2.5}$ component concentrations, and in estimating the influences of emission sources. Regarding hourly variations, the observed and simulated concentrations clearly revealed increased evening OBC concentrations due to the relatively stable atmosphere, and increased early morning fNO3 concentrations due to low temperature and high humidity, as well as remaining gaseous $HNO_3$. These factors cannot be distinguished when discrete daily concentrations are used. Continuous monitoring therefore helps in elucidating the validity of the mechanisms leading to simulated high $PM_{2.5}$ component concentrations and in improving model performance. However, it is also important to recognize the influences of uncertainties in the monitoring, particularly for components such as cSO4, OBC, and WSOC.

In terms of estimating the influences of the emission sources, we focused on dust emissions, volcanic emissions, and transboundary transport. These isolated or distant emission sources increase $PM_{2.5}$ component concentrations, but only when the airmass originates at the location of the distant source. Therefore, their influences are clearly reflected in hourly variations in concentrations. This study illustrates that regional air quality simulations can reproduce hourly variations caused by targeted emission sources. In other words, hourly variations in observed concentrations of $PM_{2.5}$ components are likely to be affected by transport from these emission sources.

Using regional air quality simulations, this study reveals that continuous monitoring data is useful for identifying key processes and emission sources that increase $PM_{2.5}$ component concentrations. Such data is likely to have various other purposes, including receptor modeling. Continuous monitoring can contribute to the development of effective strategies for suppressing ambient $PM_{2.5}$. It is therefore valuable to maintain and expand the continuous monitoring of $PM_{2.5}$ compositions.

## ACKNOWLEDGEMENT

This research was performed by the Environment Research and Technology Development Fund (JPMEERF 20165001 and JPMEERF20195003) of the Environmental Restoration and Conservation Agency of Japan. The continuous monitoring data were obtained from the Ministry of the Environment of Japan (http://www.env.go.jp/air/%20osen/pm_resultmonitoring/post_25.html).

## REFERENCES

Asano, H., Aoyama, T., Mizuno, Y., Shiraishi, Y. (2017) Highly Time-Resolved Atmospheric Observations Using a Continuous Fine Particulate Matter and Element Monitor. ACS Earth and Space Chemistry, 1(9), 580–590. https://doi.org/10.1021/acsearthspacechem.7b00090

Binkowski, F.S., Roselle, S.J. (2003) Models-3 Community Multiscale Air Quality (CMAQ) Model Aerosol Component - 1. Model Description. Journal of Geophysical Research-Atmospheres, 108(D6), 4183. https://doi.org/10.1029/2001jd001409

Byun, D., Schere, K.L. (2006) Review of the Governing Equations, Computational Algorithms, and Other Components of the Models-3 Community Multiscale Air Quality (CMAQ) Modeling System. Applied Mechanics Reviews, 59(2), 51–77. https://doi.org/10.1115/1.2128636

Cai, S.Y., Zhu, L., Wang, S.X., Wisthaler, A., Li, Q., Jiang, J.K., Hao, J.M. (2019) Time-Resolved Intermediate-Volatility and Semivolatile Organic Compound Emissions from Household Coal Combustion in Northern China. Environmental Science & Technology, 53(15), 9269–9278. https://doi.org/10.1021/acs.est.9b00734

Carter, W.P.L. (2010) Development of the SAPRC-07 Chemical Mechanism. Atmospheric Environment, 44(40), 5324–5335. https://doi.org/10.1016/j.atmosenv.2010.01.026

Chatani, S., Morino, Y., Shimadera, H., Hayami, H., Mori, Y., Sasaki, K., Kajino, M., Yokoi, T., Morikawa, T., Ohara, T. (2014) Multi-Model Analyses of Dominant Factors Influencing Elemental Carbon in Tokyo Metropolitan Area of Japan. Aerosol and Air Quality Research, 14(1), 396–405. https://doi.org/10.4209/aaqr.2013.02.0035

Chatani, S., Yamaji, K., Sakurai, T., Itahashi, S., Shimadera, H., Kitayama, K., Hayami, H. (2018) Overview of Model Inter-Comparison in Japan's Study for Reference Air Quality Modeling (J-STREAM). Atmosphere, 9(1), 19. https://doi.org/10.3390/atmos9010019

Chatani, S., Shimadera, H., Itahashi, S., Yamaji, K. (2020a) Comprehensive Analyses of Source Sensitivities and Apportionments of $PM_{2.5}$ and Ozone over Japan Via Multiple Numerical Techniques. Atmospheric Chemistry and Physics, 20(17), 10311–10329. https://doi.org/10.5194/acp-20-10311-2020

Chatani, S., Yamaji, K., Itahashi, S., Saito, M., Takigawa, M., Morikawa, T., Kanda, I., Miya, Y., Komatsu, H., Sakurai, T., Morino, Y., Nagashima, T., Kitayama, K., Shimadera, H., Uranishi, K., Fujiwara, Y., Shintani, S., Hayami, H. (2020b) Identifying Key Factors Influencing Model Performance on Ground-Level Ozone over Urban Areas in Japan through Model Inter-Comparisons. Atmospheric Environment, 223, 117255. https://doi.org/10.1016/j.atmosenv.2019.117255

Choi, Y., Kanaya, Y., Park, S.M., Matsuki, A., Sadanaga, Y., Kim, S.W., Uno, I., Pan, X., Lee, M., Kim, H., Jung, D.H. (2020) Regional Variability in Black Carbon and Carbon Monoxide Ratio from Long-Term Observations over East Asia: Assessment of Representativeness for Black Carbon (BC) and Carbon Monoxide (CO) Emission Inventories. Atmospheric Chemistry and Physics, 20(1), 83–98. https://doi.org/10.5194/acp-20-83-2020

Clappier, A., Belis, C.A., Pernigotti, D., Thunis, P. (2017) Source Apportionment and Sensitivity Analysis: Two Methodologies with Two Different Purposes. Geoscientific Model Development, 10(11), 4245–4256. https://doi.org/10.5194/gmd-10-4245-2017

Dasgupta, P.K., Campbell, S.W., Al-Horr, R.S., Ullah, S.M.R., Li, J.Z., Amalfitano, C., Poor, N.D. (2007) Conversion of Sea Salt Aerosol to $NaNO_3$ and the Production of HCl: Analysis of Temporal Behavior of Aerosol Chloride/Nitrate and Gaseous $HCl/HNO_3$ Concentrations with AIM. Atmospheric Environment, 41(20), 4242–4257. https://doi.org/10.1016/j.atmosenv.2006.09.054

Donahue, N.M., Robinson, A.L., Stanier, C.O., Pandis, S.N. (2006) Coupled Partitioning, Dilution, and Chemical Aging of Semivolatile Organics. Environmental Science & Technology, 40(8), 2635–2643. https://doi.org/10.1021/es052297c

Emery, C., Liu, Z., Russell, A.G., Odman, M.T., Yarwood, G., Kumar, N. (2017) Recommendations on Statistics and Benchmarks to Assess Photochemical Model Performance. Journal of the Air & Waste Management Association, 67(5), 582–598. https://doi.org/10.1080/10962247.2016.1265027

Foroutan, H., Young, J., Napelenok, S., Ran, L., Appel, K.W., Gilliam, R.C., Pleim, J.E. (2017) Development and Evaluation of a Physics-Based Windblown Dust Emission Scheme Implemented in the CMAQ Modeling System. Journal of Advances in Modeling Earth Systems, 9(1), 585–608. https://doi.org/10.1002/2016ms000823

Fountoukis, C., Nenes, A. (2007) Isorropia Ii: A Computation-

ally Efficient Thermodynamic Equilibrium Model for $K^+$ - $Ca^{2+}$ - $Mg^{2+}$ - $NH_4^+$ - $Na^+$ - $SO_4^{2-}$ - $NO_3^-$ - $Cl^-$ - $H_2O$ Aerosols. Atmospheric Chemistry and Physics, 7(17), 4639–4659. https://doi.org/10.5194/acp-7-4639-2007

Fu, X., Wang, S.X., Zhao, B., Xing, J., Cheng, Z., Liu, H., Hao, J.M. (2013) Emission Inventory of Primary Pollutants and Chemical Speciation in 2010 for the Yangtze River Delta Region, China. Atmospheric Environment, 70, 39–50. https://doi.org/10.1016/j.atmosenv.2012.12.034

Ikemori, F., Uranishi, K., Sato, T., Fujihara, M., Hasegawa, H., Sugata, S. (2021) Time-Resolved Characterization of Organic Compounds in $PM_{2.5}$ Collected at Oki Island, Japan, Affected by Transboundary Pollution of Biomass and Non-Biomass Burning from Northeast China. Science of the Total Environment, 750, 142183. https://doi.org/10.1016/j.scitotenv.2020.142183

Itahashi, S., Uno, I., Osada, K., Kamiguchi, Y., Yamamoto, S., Tamura, K., Wang, Z., Kurosaki, Y., Kanaya, Y. (2017) Nitrate Transboundary Heavy Pollution over East Asia in Winter. Atmospheric Chemistry and Physics, 17(6), 3823–3843. https://doi.org/10.5194/acp-17-3823-2017

Itahashi, S., Yamaji, K., Chatani, S., Hayami, H. (2018a) Refinement of Modeled Aqueous-Phase Sulfate Production Via the Fe- and Mn-Catalyzed Oxidation Pathway. Atmosphere, 9(4), 132. https://doi.org/10.3390/atmos9040132

Itahashi, S., Yamaji, K., Chatani, S., Hisatsune, K., Saito, S., Hayami, H. (2018b) Model Performance Differences in Sulfate Aerosol in Winter over Japan Based on Regional Chemical Transport Models of CMAQ and CAMx. Atmosphere, 9(12), 488. https://doi.org/10.3390/atmos9120488

Itahashi, S., Yamaji, K., Chatani, S., Hayami, H. (2019) Differences in Model Performance and Source Sensitivities for Sulfate Aerosol Resulting from Updates of the Aqueous- and Gas-Phase Oxidation Pathways for a Winter Pollution Episode in Tokyo, Japan. Atmosphere, 10(9), 544. https://doi.org/10.3390/atmos10090544

Itahashi, S., Wang, Z., Yumimoto, K., Uno, I. (2020a) Drastic Changes of $PM_{2.5}$ Trans-Boundary Pollution over Japan Due to COVID-19 Lockdown in China. Journal of Japan Society for Atmospheric Environment/Taiki Kankyo Gakkaishi, 55(6), 239–247. https://doi.org/10.11298/taiki.55.239

Itahashi, S., Yamaji, K., Chatani, S., Kitayama, K., Morino, Y., Nagashima, T., Saito, M., Takigawa, M., Morikawa, T., Kanda, I., Miya, Y., Komatsu, H., Sakurai, T., Shimadera, H., Uranishi, K., Fujiwara, Y., Hashimoto, T., Hayami, H. (2020b) Model Performance Differences in Fine-Mode Nitrate Aerosol During Wintertime over Japan in the J-STREAM Model Inter-Comparison Study. Atmosphere, 11(5), 511. https://doi.org/10.3390/atmos11050511

Janssens-Maenhout, G., Crippa, M., Guizzardi, D., Dentener, F., Muntean, M., Pouliot, G., Keating, T., Zhang, Q., Kurokawa, J., Wankmuller, R., van der Gon, H.D., Kuenen, J.J.P., Klimont, Z., Frost, G., Darras, S., Koffi, B., Li, M. (2015) HTAP_V2.2: A Mosaic of Regional and Global Emission Grid Maps for 2008 and 2010 to Study Hemispheric Transport of Air Pollution. Atmospheric Chemistry and Physics, 15(19), 11411–11432. https://doi.org/10.5194/acp-15-11411-2015

Kajino, M., Sato, K., Inomata, Y., Ueda, H. (2013) Source-Receptor Relationships of Nitrate in Northeast Asia and Influence of Sea Salt on the Long-Range Transport of Nitrate. Atmospheric Environment, 79, 67–78. https://doi.org/10.1016/j.atmosenv.2013.06.024

Kajino, M., Hagino, H., Fujitani, Y., Morikawa, T., Fukui, T., Onishi, K., Okuda, T., Kajikawa, T., Igarashi, Y. (2020) Modeling Transition Metals in East Asia and Japan and Its Emission Sources. Geohealth, 4(9), e2020GH000259. https://doi.org/10.1029/2020gh000259

Kanaya, Y., Yamaji, K., Miyakawa, T., Taketani, F., Zhu, C., Choi, Y., Komazaki, Y., Ikeda, K., Kondo, Y., Klimont, Z. (2020) Rapid Reduction in Black Carbon Emissions from China: Evidence from 2009–2019 Observations on Fukue Island, Japan. Atmospheric Chemistry and Physics, 20(11), 6339–6356. https://doi.org/10.5194/acp-20-6339-2020

Kelly, J.T., Bhave, P.V., Nolte, C.G., Shankar, U., Foley, K.M. (2010) Simulating Emission and Chemical Evolution of Coarse Sea-Salt Particles in the Community Multiscale Air Quality (CMAQ) Model. Geoscientific Model Development, 3(1), 257–273. https://doi.org/10.5194/gmd-3-257-2010

Kojima, S., Michikawa, T., Matsui, K., Ogawa, H., Yamazaki, S., Nitta, H., Takami, A., Ueda, K., Tahara, Y., Yonemoto, N., Nonogi, H., Nagao, K., Ikeda, T., Sato, N., Tsutsui, H. (2020) Association of Fine Particulate Matter Exposure with Bystander-Witnessed out-of-Hospital Cardiac Arrest of Cardiac Origin in Japan. JAMA Network Open, 3(4), e203043. https://doi.org/10.1001/jamanetworkopen.2020.3043

Kondo, Y., Miyazaki, Y., Takegawa, N., Miyakawa, T., Weber, R.J., Jimenez, J.L., Zhang, Q., Worsnop, D.R. (2007) Oxygenated and Water-Soluble Organic Aerosols in Tokyo. Journal of Geophysical Research-Atmospheres, 112(D1), D01203. https://doi.org/10.1029/2006jd007056

Li, Y.Y., Chang, M.A., Ding, S.S., Wang, S.W., Ni, D., Hu, H.T. (2017) Monitoring and Source Apportionment of Trace Elements in $PM_{2.5}$: Implications for Local Air Quality Management. Journal of Environmental Management, 196, 16–25. https://doi.org/10.1016/j.jenvman.2017.02.059

Liu, H., Man, H.Y., Cui, H.Y., Wang, Y.J., Deng, F.Y., Wang, Y., Yang, X.F., Xiao, Q., Zhang, Q., Ding, Y., He, K.B. (2017) An Updated Emission Inventory of Vehicular Vocs and Ivocs in China. Atmospheric Chemistry and Physics, 17(20), 12709–12724. https://doi.org/10.5194/acp-17-12709-2017

Ministry of the Environment (2020) https://www.env.go.jp/air/osen/index.html (Last access: December 3rd, 2020).

Miyazaki, Y., Kondo, Y., Takegawa, N., Komazaki, Y., Fukuda, M., Kawamura, K., Mochida, M., Okuzawa, K., Weber, R.J. (2006) Time-Resolved Measurements of Water-Soluble Organic Carbon in Tokyo. Journal of Geophysical Research-Atmospheres, 111(D23), D23206. https://doi.org/10.1029/2006jd007125

Morino, Y., Nagashima, T., Sugata, S., Sato, K., Tanabe, K., Noguchi, T., Takami, A., Tanimoto, H., Ohara, T. (2015) Verification of Chemical Transport Models for $PM_{2.5}$ Chemical Composition Using Simultaneous Measurement Data over Japan. Aerosol and Air Quality Research, 15(5), 2009–2023. https://doi.org/10.4209/aaqr.2015.02.0120

Morino, Y., Chatani, S., Tanabe, K., Fujitani, Y., Morikawa, T.,

Takahashi, K., Sato, K., Sugata, S. (2018) Contributions of Condensable Particulate Matter to Atmospheric Organic Aerosol over Japan. Environmental Science & Technology, 52(15), 8456–8466. https://doi.org/10.1021/acs.est.8b01285

Murphy, B.N., Woody, M.C., Jimenez, J.L., Carlton, A.M.G., Hayes, P.L., Liu, S., Ng, N.L., Russell, L.M., Setyan, A., Xu, L., Young, J., Zaveri, R.A., Zhang, Q., Pye, H.O.T. (2017) Semivolatile POA and Parameterized Total Combustion SOA in Cmaqv5.2: Impacts on Source Strength and Partitioning. Atmospheric Chemistry and Physics, 17(18), 11107–11133. https://doi.org/10.5194/acp-17-11107-2017

Nakatsubo, R., Horie, Y., Takimoto, M., Matsumura, C., Hiraki, T. (2018) Analysis of Hourly Observation Data of $PM_{2.5}$ Chemical Components at a Coastal Area in Seto Inland Sea. Earozoru Kenkyu, 33(3), 175–182. https://doi.org/10.11203/jar.33.175

Nenes, A., Pandis, S.N., Weber, R.J., Russell, A. (2020) Aerosol Ph and Liquid Water Content Determine When Particulate Matter Is Sensitive to Ammonia and Nitrate Availability. Atmospheric Chemistry and Physics, 20(5), 3249–3258. https://doi.org/10.5194/acp-20-3249-2020

Osada, K., Kamiguchi, Y., Yamamoto, S., Kuwahara, S., Pan, X., Hara, Y., Uno, I. (2016) Comparison of Ionic Concentrations on Size-Segregated Atmospheric Aerosol Particles Based on a Denuder-Filter Method and a Continuous Dichotomous Aerosol Chemical Speciation Analyzer (ACSA-12). Earozoru Kenkyu, 31(3), 203–209. https://doi.org/10.11203/jar.31.203

Otte, T.L., Pleim, J.E. (2010) The Meteorology-Chemistry Interface Processor (MCIP) for the CMAQ Modeling System: Updates through Mcipv3.4.1. Geoscientific Model Development, 3(1), 243–256. https://doi.org/10.5194/gmd-3-243-2010

Pan, X.L., Ge, B.Z., Wang, Z., Tian, Y., Liu, H., Wei, L.F., Yue, S.Y., Uno, I., Kobayashi, H., Nishizawa, T., Shimizu, A., Fu, P.Q., Wang, Z.F. (2019) Synergistic Effect of Water-Soluble Species and Relative Humidity on Morphological Changes in Aerosol Particles in the Beijing Megacity During Severe Pollution Episodes. Atmospheric Chemistry and Physics, 19(1), 219–232. https://doi.org/10.5194/acp-19-219-2019

Pleim, J.E. (2007) A Combined Local and Nonlocal Closure Model for the Atmospheric Boundary Layer. Part I: Model Description and Testing. Journal of Applied Meteorology and Climatology, 46(9), 1383–1395. https://doi.org/10.1175/jam2539.1

Ramboll Environ (2016) CAMx User's Guide Version 6.40. http://www.camx.com/files/camxusersguide_v6-40.pdf

Robinson, A.L., Donahue, N.M., Shrivastava, M.K., Weitkamp, E.A., Sage, A.M., Grieshop, A.P., Lane, T.E., Pierce, J.R., Pandis, S.N. (2007) Rethinking Organic Aerosols: Semivolatile Emissions and Photochemical Aging. Science, 315(5816), 1259. https://doi.org/10.1126/science.1133061

Saito, S., Hoshi, J., Ikemori, F., Osada, K. (2020) Comparison of Water-Soluble Organic Carbon in $PM_{2.5}$ Obtained by Filter Analysis and Continuous Dichotomous Aerosol Chemical Speciation Analyzer. Journal of Japan Society for Atmospheric Environment/Taiki Kankyo Gakkaishi, 55(3), 150–158. https://doi.org/10.11298/taiki.55.150

Shimadera, H., Hayami, H., Chatani, S., Morino, Y., Mori, Y., Morikawa, T., Yamaji, K., Ohara, T. (2014) Sensitivity Analyses of Factors Influencing CMAQ Performance for Fine Particulate Nitrate. Journal of the Air & Waste Management Association, 64(4), 374–387. https://doi.org/10.1080/10962247.2013.778919

Sudo, K., Takahashi, M., Kurokawa, J., Akimoto, H. (2002) CHASER: A Global Chemical Model of the Troposphere - 1. Model Description. Journal of Geophysical Research-Atmospheres, 107(D17), 4339. https://doi.org/10.1029/2001jd001113

Uno, I., Osada, K., Yumimoto, K., Wang, Z., Itahashi, S., Pan, X.L., Hara, Y., Kanaya, Y., Yamamoto, S., Fairlie, T.D. (2017a) Seasonal Variation of Fine- and Coarse-Mode Nitrates and Related Aerosols over East Asia: Synergetic Observations and Chemical Transport Model Analysis. Atmospheric Chemistry and Physics, 17(23), 14181–14197. https://doi.org/10.5194/acp-17-14181-2017

Uno, I., Osada, K., Yumimoto, K., Wang, Z., Itahashi, S., Pan, X.L., Hara, Y., Yamamoto, S., Nishizawa, T. (2017b) Importance of Long-Range Nitrate Transport Based on Long-Term Observation and Modeling of Dust and Pollutants over East Asia. Aerosol and Air Quality Research, 17(12), 3052–3064. https://doi.org/10.4209/aaqr.2016.11.0494

Uno, I., Wang, Z., Itahashi, S., Yumimoto, K., Yamamura, Y., Yoshino, A., Takami, A., Hayasaki, M., Kim, B.-G. (2020) Paradigm Shift in Aerosol Chemical Composition over Regions Downwind of China. Scientific Reports, 10(1), 6450. https://doi.org/10.1038/s41598-020-63592-6

Uranishi, K., Ikemori, F., Nakatsubo, R., Shimadera, H., Kondo, A., Kikutani, Y., Asano, K., Sugata, S. (2017) Identification of Biased Sectors in Emission Data Using a Combination of Chemical Transport Model and Receptor Model. Atmospheric Environment, 166, 166–181. https://doi.org/10.1016/j.atmosenv.2017.06.039

Yamaji, K., Chatani, S., Itahashi, S., Saito, M., Takigawa, M., Morikawa, T., Kanda, I., Miya, Y., Komatsu, H., Sakurai, T., Morino, Y., Kitayama, K., Nagashima, T., Shimadera, H., Uranishi, K., Fujiwara, Y., Hashimoto, T., Sudo, K., Misaki, T., Hayami, H. (2020) Model Inter-Comparison for $PM_{2.5}$ Components over Urban Areas in Japan in the J-STREAM Framework. Atmosphere, 11(3), 222. https://doi.org/10.3390/atmos11030222

Yan, C.Q., Zheng, M., Sullivan, A.P., Bosch, C., Desyaterik, Y., Andersson, A., Li, X.Y., Guo, X.S., Zhou, T., Gustafsson, O., Collett, J.L. (2015) Chemical Characteristics and Light-Absorbing Property of Water-Soluble Organic Carbon in Beijing: Biomass Burning Contributions. Atmospheric Environment, 121, 4–12. https://doi.org/10.1016/j.atmosenv.2015.05.005

Ye, S.Q., Ma, T., Duan, F.K., Li, H., He, K.B., Xia, J., Yang, S., Zhu, L.D., Ma, Y.L., Huang, T., Kimoto, T. (2019) Characteristics and Formation Mechanisms of Winter Haze in Changzhou, a Highly Polluted Industrial City in the Yangtze River Delta, China. Environmental Pollution, 253, 377–383. https://doi.org/10.1016/j.envpol.2019.07.011

Zhang, L., Brook, J.R., Vet, R. (2003) A Revised Parameterization for Gaseous Dry Deposition in Air-Quality Models.

Atmospheric Chemistry and Physics, 3(6), 2067–2082. https://doi.org/10.5194/acp-3-2067-2003

Zhang, X.X., Sharratt, B., Liu, L.Y., Wang, Z.F., Pan, X.L., Lei, J.Q., Wu, S.X., Huang, S.Y., Guo, Y.H., Li, J., Tang, X., Yang, T., Tian, Y., Chen, X.S., Hao, J.Q., Zheng, H.T., Yang, Y.Y., Lyu, Y.L. (2018) East Asian Dust Storm in May 2017: Observations, Modelling, and Its Influence on the Asia-Pacific Region. Atmospheric Chemistry and Physics, 18(11), 8353–8371. https://doi.org/10.5194/acp-18-8353-2018

## SUPPLEMENTARY MATERIALS

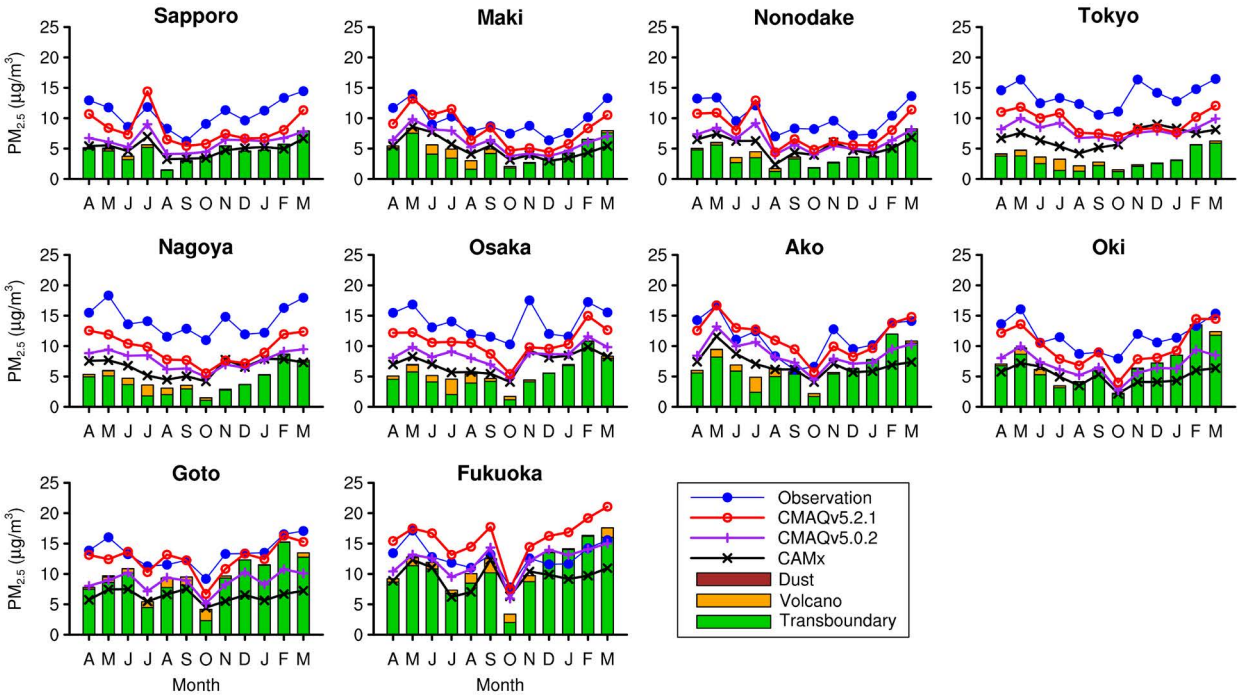


(a) $PM_{2.5}$: ambient fine particulate matter < 2.5 μm

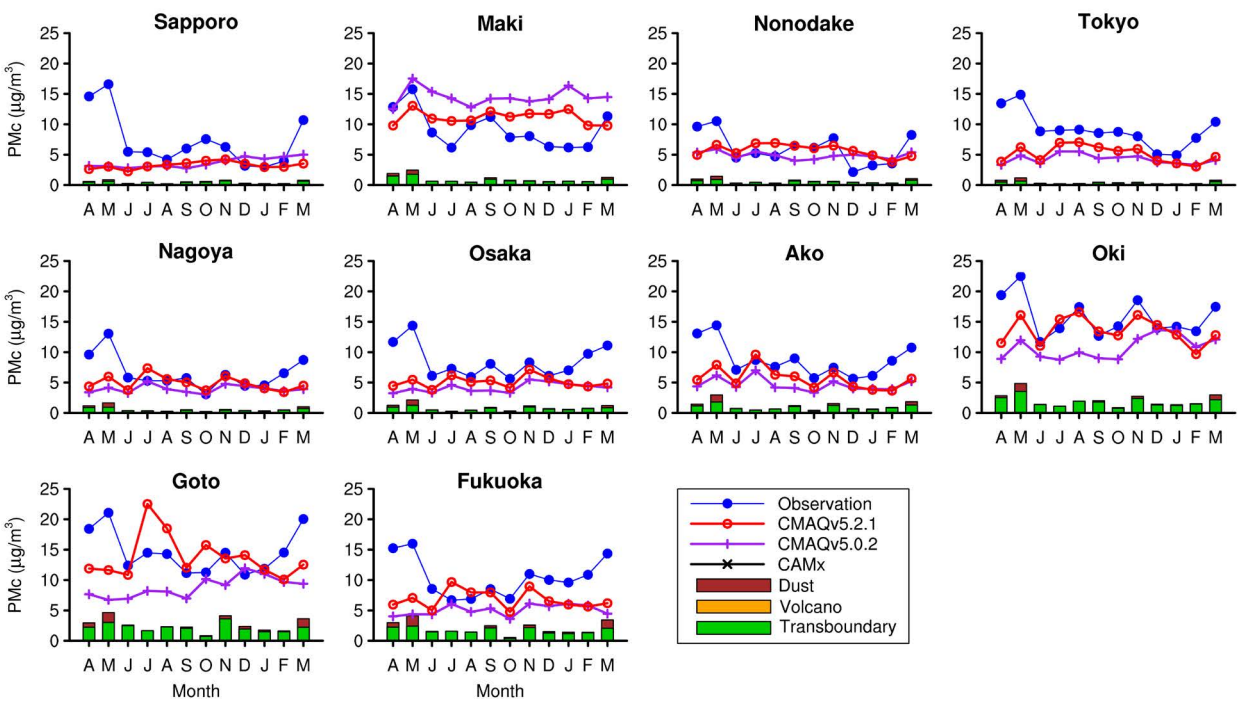


(b) PMc: coarse-fraction PM

**Fig. S1.** Air quality parameters at the ten ACSA-14 stations, giving the observed and simulated monthly mean concentrations and source sensitivities. The values were averaged over all hours in each month. Concentrations are denoted by lines and markers; sensitivities by cumulative bars. Models used: CMAQ v. 5.2.1 and 5.0.2, and CAMx.

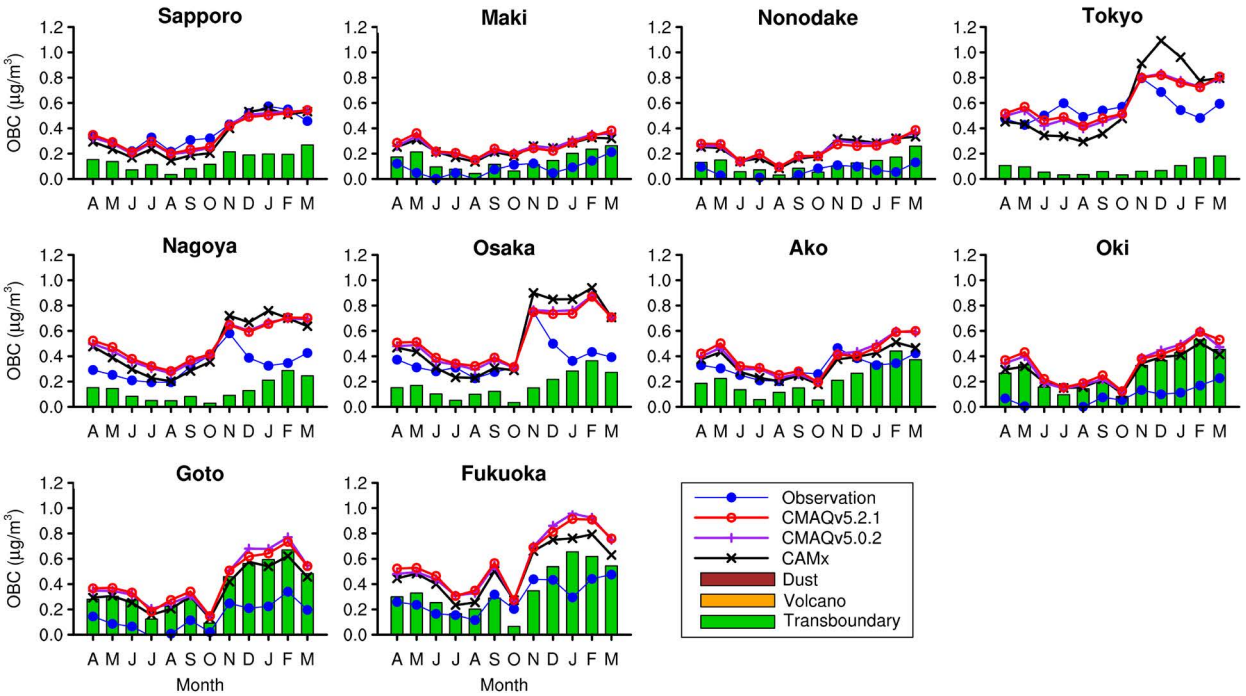


(c) OBC: fine-fraction contents of optically measured black carbon

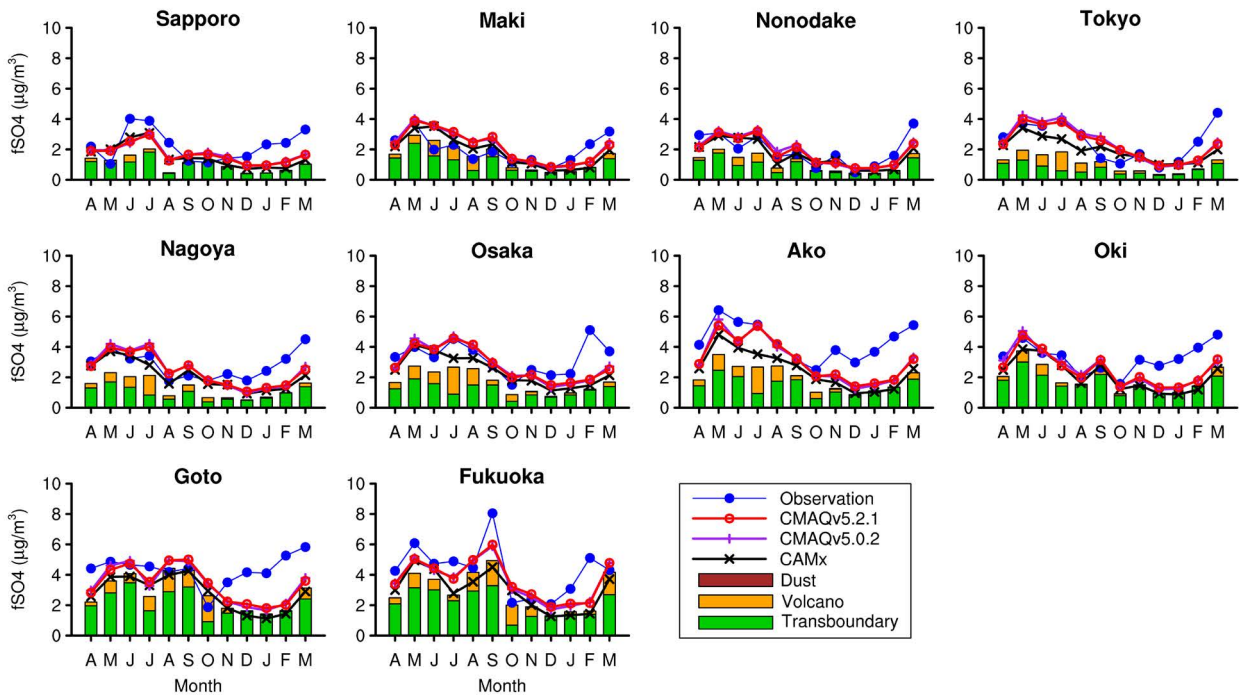


(d) fSO4: fine-fraction contents of $SO_4^{2-}$

**Fig. S1.** Continued.

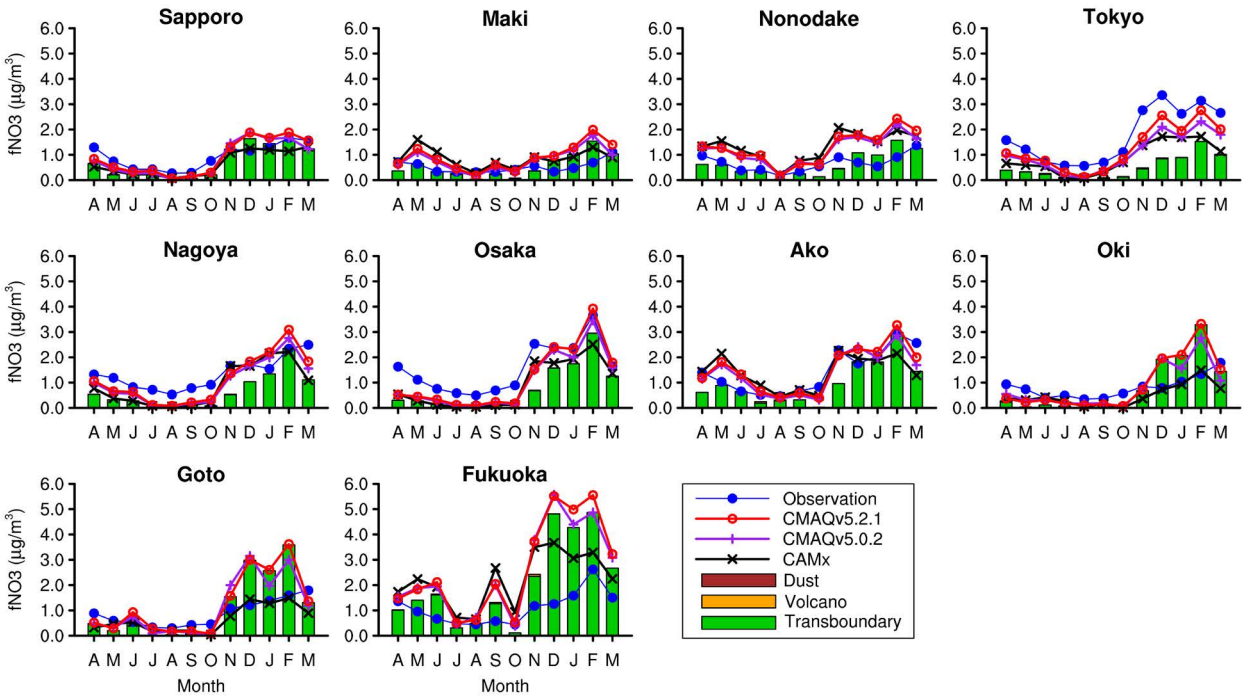


(e) fNO3: fine-fraction contents of $NO_3^-$

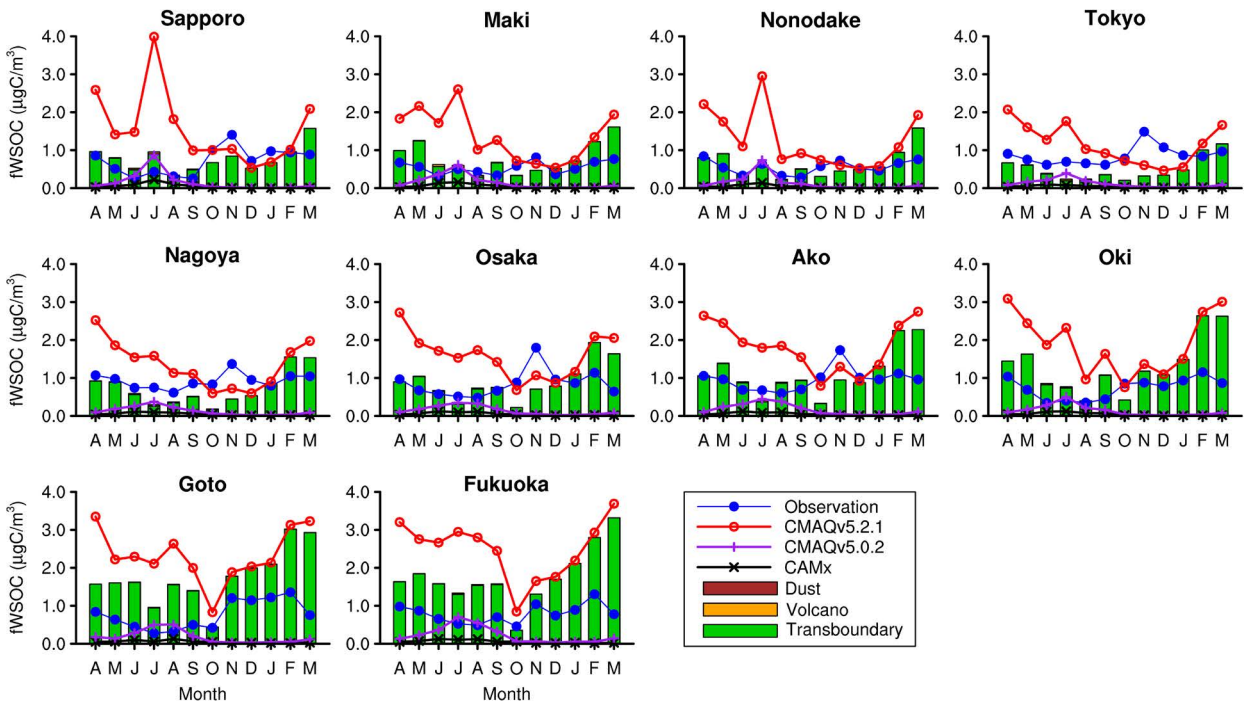


(f) fWSOC: fine-fraction contents of water-soluble organic carbon

**Fig. S1.** Continued.

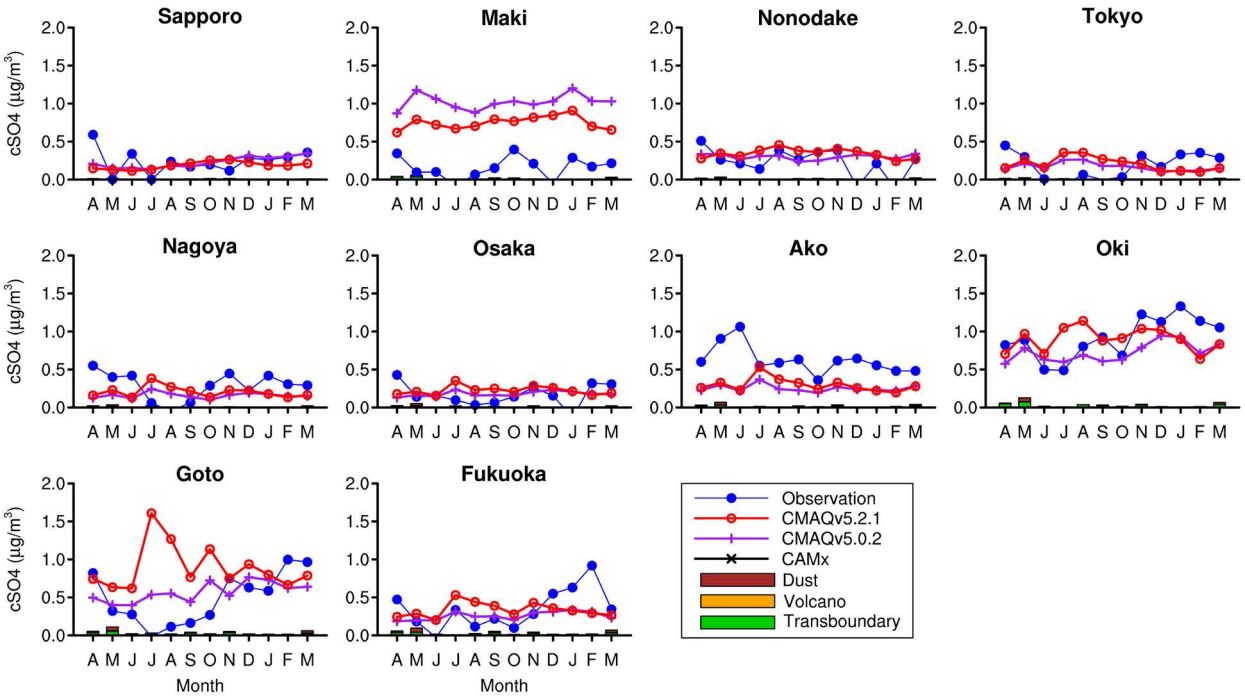


(g) cSO4: coarse-fraction contents of $SO_4^{2-}$

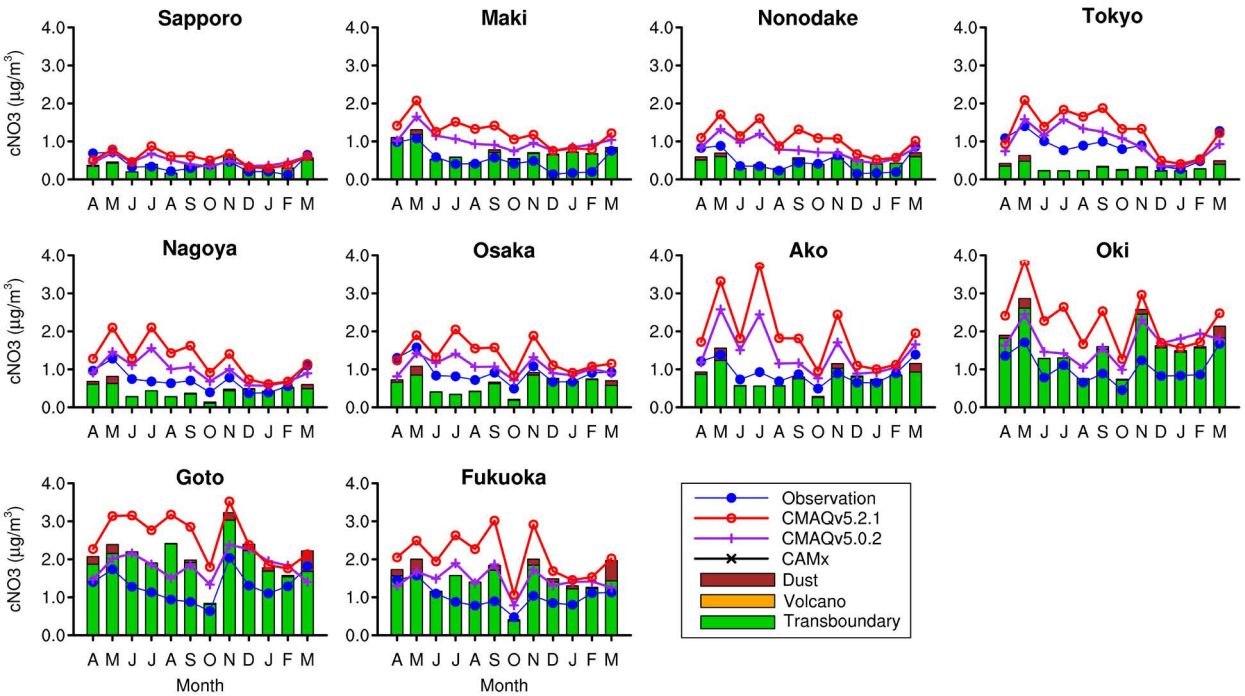


(h) cNO3: coarse-fraction contents of $NO_3^-$

**Fig. S1.** Continued.

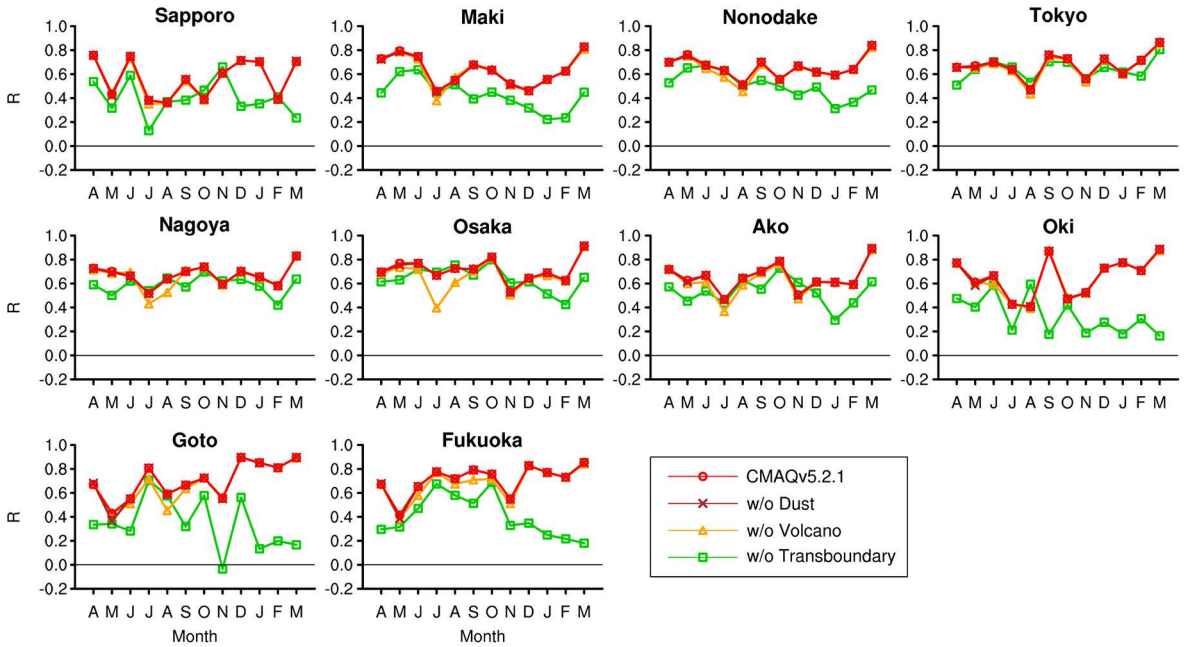


(a) $PM_{2.5}$: ambient fine particulate matter < 2.5 μm

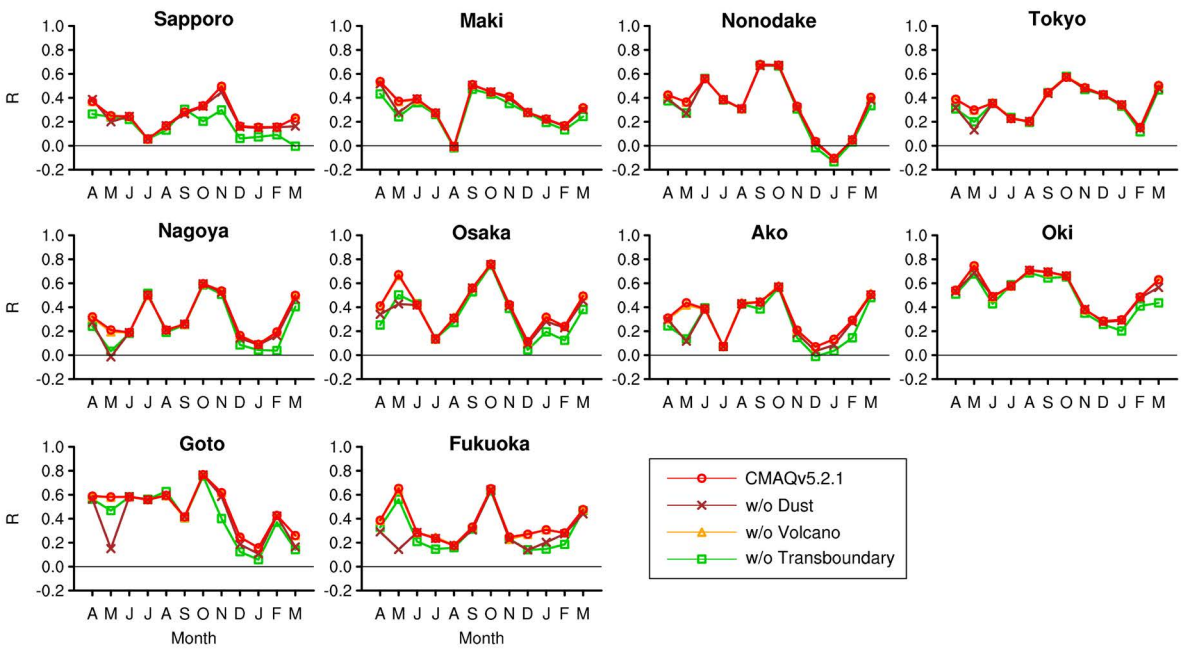


(b) PMc: coarse-fraction PM

**Fig. S2.** Monthly variation in correlation coefficients of air quality parameters at the ten ACSA-14 stations, based on hourly concentrations of particulate matter (PM) and its components simulated using CMAQ v. 5.2.1 in the base and sensitivity simulations. w/o: without.

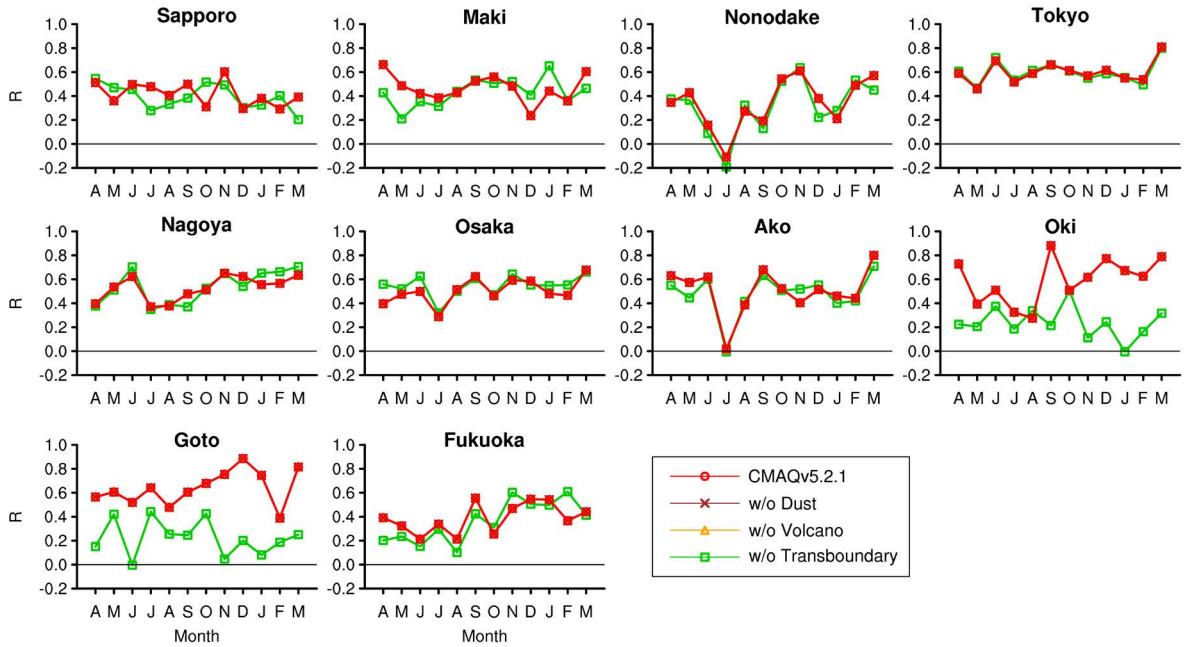


(c) OBC: fine-fraction contents of optically measured black carbon

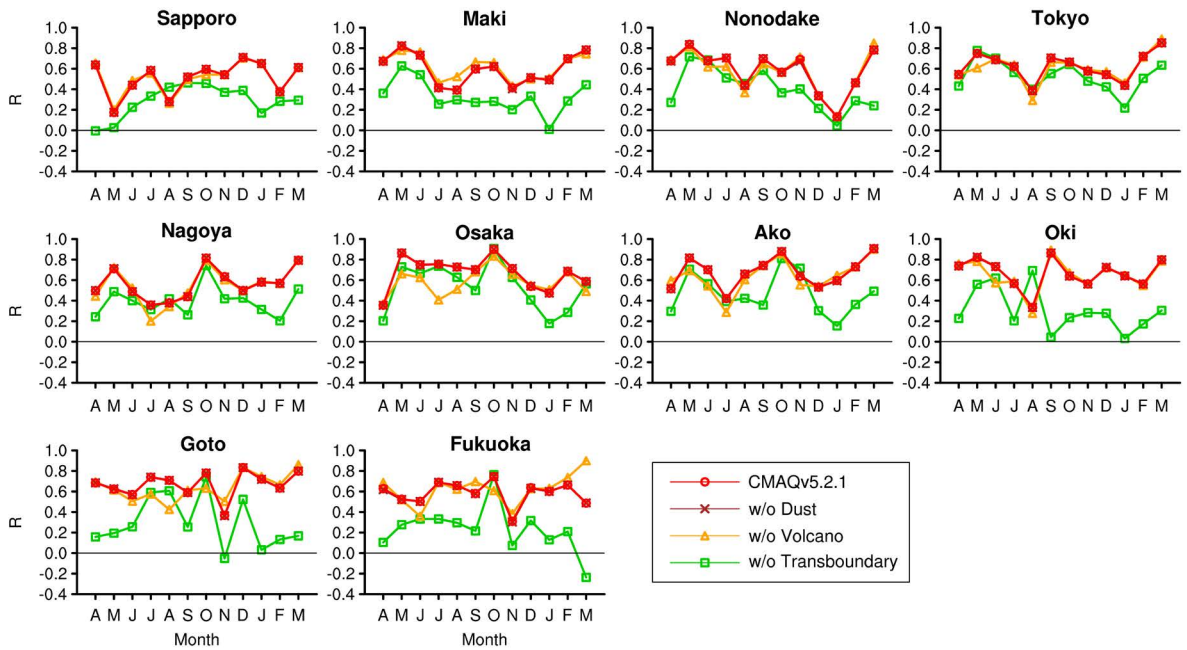


(d) fSO4: fine-fraction contents of $SO_4^{2-}$

**Fig. S2.** Continued.

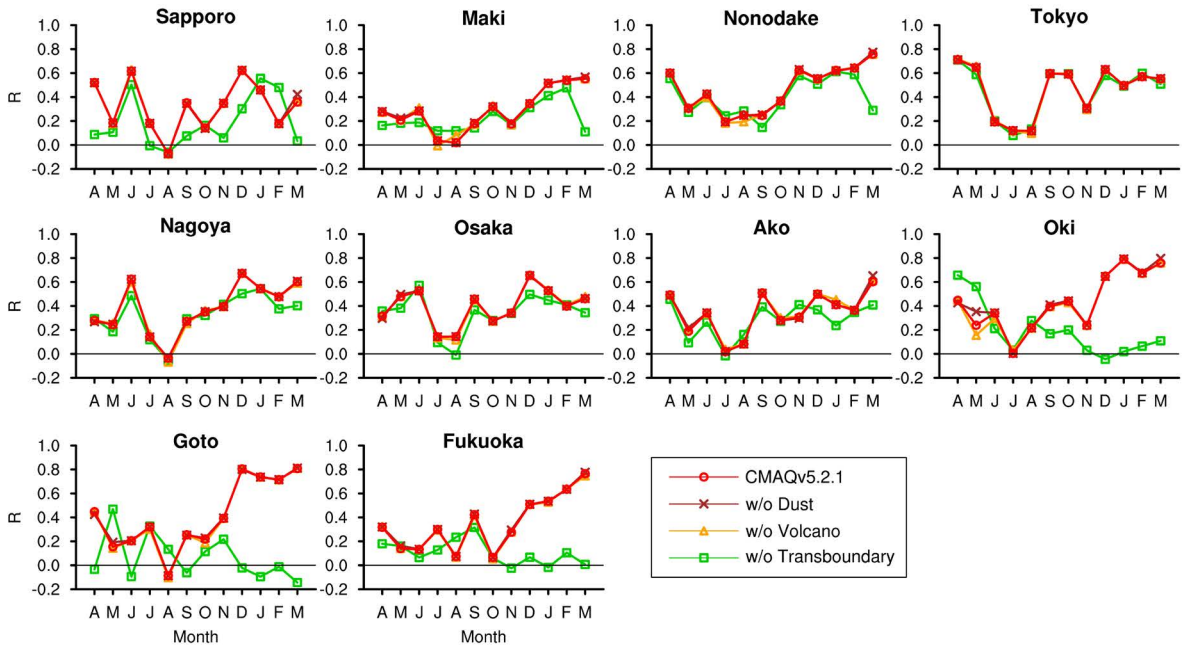


(e) fNO3: fine-fraction contents of $NO_3^-$

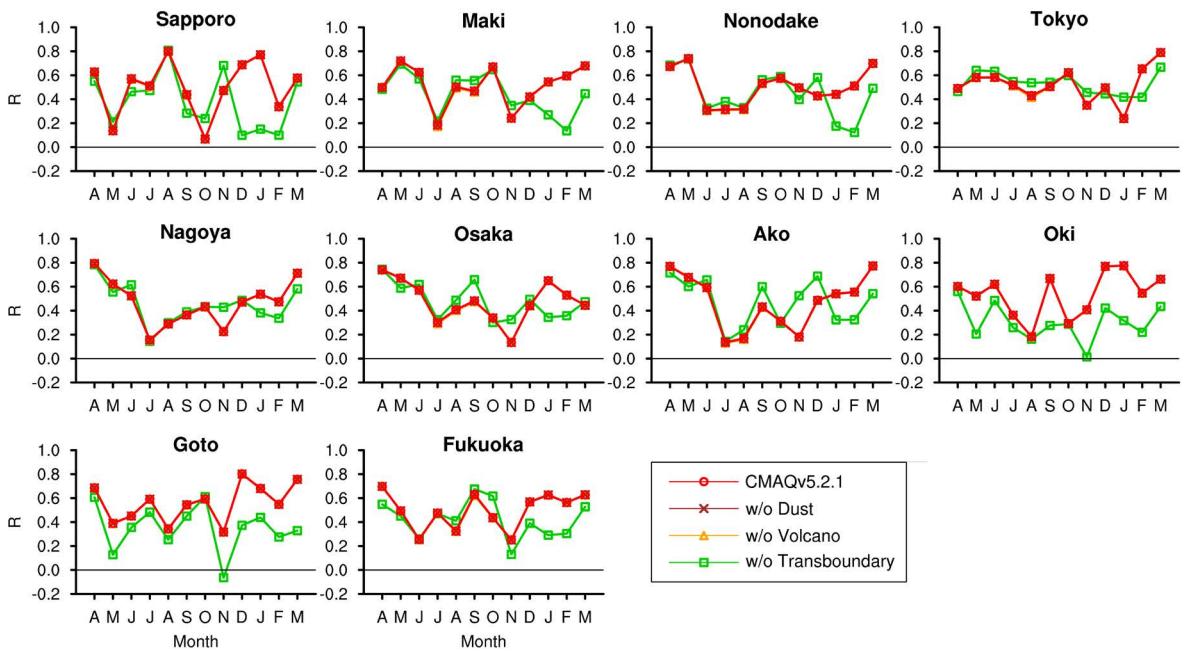


(f) fWSOC: fine-fraction contents of water-soluble organic carbon

**Fig. S2.** Continued.

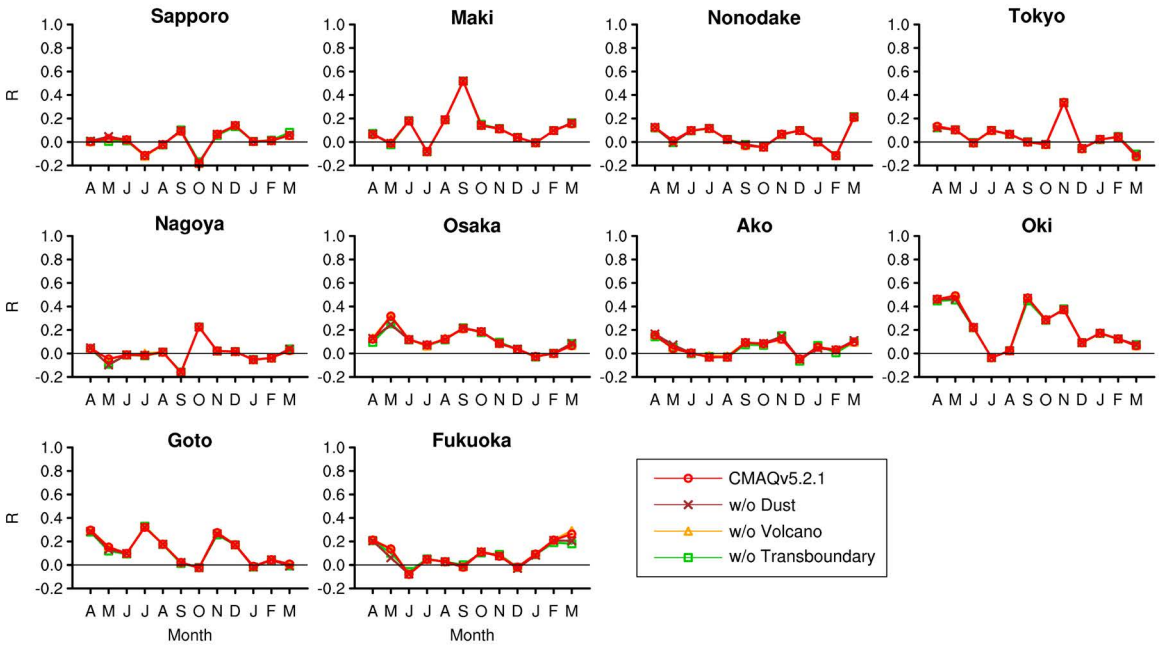


(g) cSO4: coarse-fraction contents of $SO_4^{2-}$

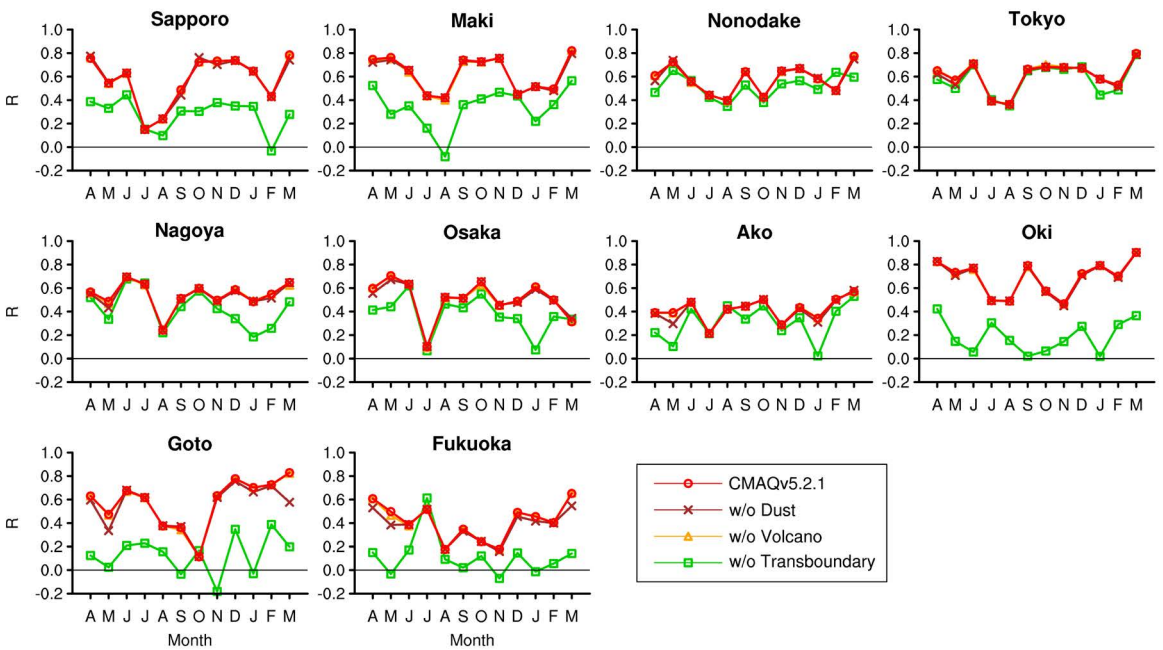


(h) cNO3: coarse-fraction contents of $NO_3^-$

**Fig. S2.** Continued.

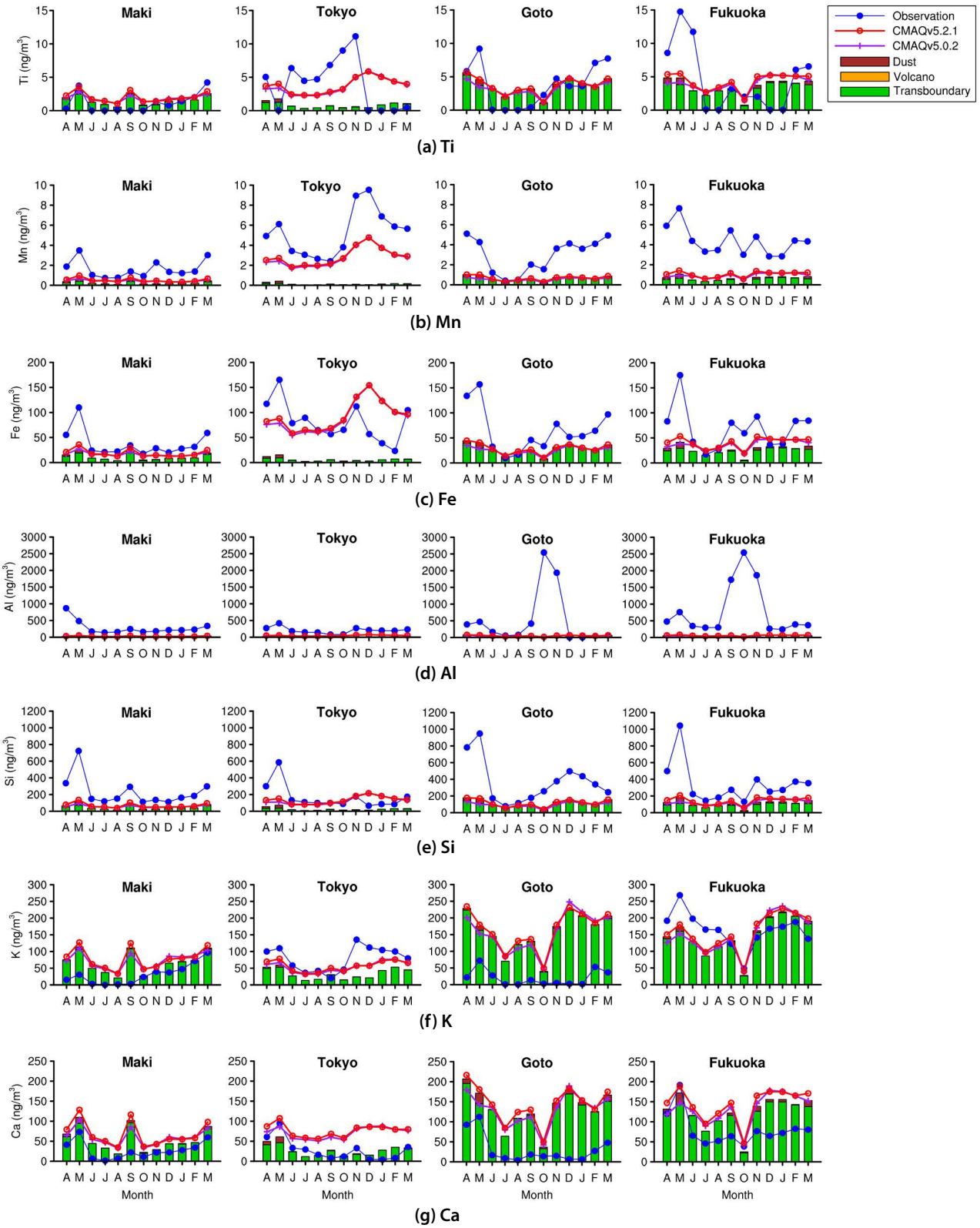


**Fig. S3.** Air quality parameters at the four PX-375 stations, giving the observed and simulated monthly mean concentrations and source sensitivities. The values were averaged over all hours in each month. Concentrations are denoted by lines and markers; sensitivities by cumulative bars. Models used: CMAQ v. 5.2.1 and 5.0.2.

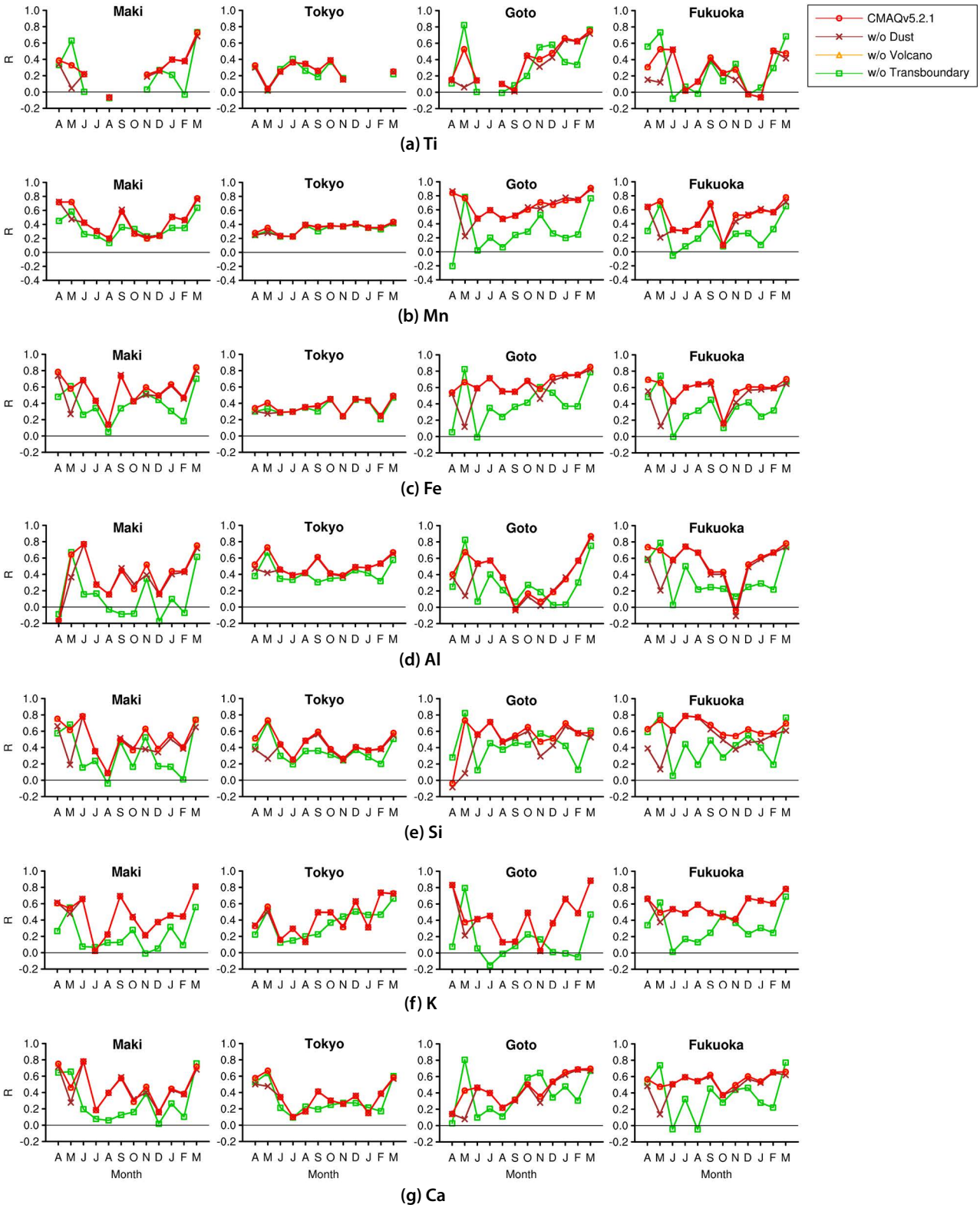


**Fig. S4.** Monthly variation in correlation coefficients of air quality parameters at the four PX-375 stations, based on hourly concentrations of metals simulated using CMAQ v. 5.2.1 in the base and sensitivity simulations. w/o: without.